

1 **Regional Magma Plumbing and emplacement mechanisms of the**

2 **Faroe-Shetland Sill Complex:**

3 **Implications for magma transport and petroleum systems within sedimentary basins**

4
5 **Nick Schofield¹, Simon Holford², John Millett¹, David Brown³, David Jolley¹, Simon**
6 **Passey⁴, Dave Muirhead¹, Clayton Grove⁵, Craig Magee⁶, Joanne Murray⁷, Malcolm**
7 **Hole¹, Christopher Jackson⁶, Carl Stevenson⁷**

8 *¹Geology and Petroleum Geology, School of Geosciences, University of Aberdeen, Meston Building, Aberdeen, AB24*
9 *3UE, UK*

10 *²Australian School of Petroleum, University of Adelaide, SA 5005, Australia*

11 *³School of Geographical and Earth Sciences, University of Glasgow, Gregory Building, Lilybank Gardens, Glasgow,*
12 *G12 8QQ, UK*

13 *⁴CASP, West Building, 181A Huntingdon Road, Cambridge, CB3 0DH, UK*

14 *⁵OMV (U.K.), 62 Buckingham Gate, London, SW1E 6AJ, UK*

15 *⁶Basins Research Group (BRG), Department of Earth Science and Engineering, Imperial College, London, SW7 2BP,*
16 *UK*

17 *⁷Earth Sciences, University of Birmingham, B15 2TT, UK*

18 *Corresponding author – e-mail: n.schofield@abdn.ac.uk Tel: 01224 272096*

19
20 **Abstract**

21 The movement of magma through the shallow crust and the impact of subsurface sill complexes
22 on the hydrocarbon systems of prospective sedimentary basins has long been an area of interest
23 and debate. Based on 3D seismic reflection and well data, we present a regional analysis of the
24 emplacement and magmatic plumbing system of the Palaeogene Faroe-Shetland Sill Complex
25 (FSSC), which is intruded into the Mesozoic and Cenozoic sequences of the Faroe-Shetland Basin
26 (FSB). Identification of magma flow directions through detailed seismic interpretation of

27 approximately 100 sills indicates that the main magma input zones into the FSB were controlled
28 primarily by the NE-SW basin structure that compartmentalise the FSB into its constituent sub-
29 basins.

30 An analysis of well data shows that potentially up to 88% of sills in the FSSC are <40 m in
31 thickness, and thus below the vertical resolution limit of seismic data at depths at which most sills
32 occur. This resolution limitation suggests that caution needs to be exercised when interpreting
33 magmatic systems from seismic data alone, as a large amount of intrusive material could potentially
34 be missed.

35 The interaction of the FSSC with the petroleum systems of the FSB is not well understood.
36 Given the close association between the FSSC and potential petroleum migration routes into
37 some of the oil/gas fields (e.g. Tormore), the role the intrusions may have played in
38 compartmentalization of basin fill needs to be taken fully into account to further unlock the future
39 petroleum potential of the FSB.

40

41 Keywords: Faroe-Shetland Basin, 3D seismic interpretation, Sills, Magma, Volcanic Rifted Margins

42

43

Introduction

44 In recent years, our understanding of sub-volcanic magmatic plumbing systems within
45 sedimentary basins has been revolutionised by the study of petroleum industry 3D seismic
46 reflection datasets. In particular, 3D seismic reflection data have provided important insights into
47 sheet intrusion geometry, emplacement mechanisms, and magma flow between multiple intrusions
48 within sill-complexes in basins located along the Norwegian Margin, the NE Atlantic Margin, and
49 offshore Australia (e.g. Davies et al., 2002; Smallwood and Maresh, 2002; Thomson and Hutton,
50 2004; Archer et al. 2005; Planke et al., 2005; Hansen and Cartwright, 2006; Thomson and
51 Schofield, 2008; Jackson et al. 2013; Magee et al. 2013a, b, c).

52 It is widely acknowledged that magmatic processes play a key role in continental breakup
53 (e.g. Afar; Wright et al. 2012) and that magmatic sheet (sill) intrusion contributes significantly to
54 the upper crustal magma transport network. Interconnected sills may also represent a unique type
55 of magma chamber (Cartwright and Hansen, 2006; Marsh, 2004), whereby the magma hosted
56 within the sill complex forms an interconnected body of magma, which could serve the same
57 purpose as a single magma chamber.

58 Whilst previous seismic interpretation-based studies have addressed aspects of the
59 magmatic plumbing system with regard to how networks of interconnected sills link (Cartwright
60 and Hansen, 2006), how sills grow and how they exploit structural/stratigraphic anisotropy
61 (Thomson and Hutton, 2004; Schofield et al. 2012a), most of this work has been conducted using
62 isolated datasets, often due to limited data availability. These studies are typically focused on scales
63 of over 10s of km (e.g. Thomson and Schofield; 2008; Schofield et al. 2012; Planke et al. 2005);
64 however, no basin scale study (over 100s of km) has been undertaken.

65 The Faroe-Shetland Basin (FSB) was a site of extensive extrusive and intrusive igneous
66 activity during the Palaeogene, as a result of the impingement of the proto-Icelandic Plume and the
67 onset of sea floor spreading (e.g. Saunders et al. 1997; Passey and Hitchen, 2011). The basin was
68 heavily intruded by a series of sill intrusions, and these provide an excellent opportunity to
69 understand the development of shallow crustal, rift-related magmatism within a sedimentary basin.
70 The FSB also arguably represents one of the last major frontier exploration areas within the
71 United Kingdom Continental Shelf (UKCS), and contains several large producing fields (e.g. Clair,
72 Foinaven, Schiehallion). For this reason, unlike many volcanic margin basins, the FSB is covered
73 extensively by 3D seismic data, such as the high quality regional 3D seismic survey, the FSB
74 MegaSurvey Plus, which covers a surface area of ~24,000 km².

75 This study presents a detailed, seismic-based characterisation of the Faroe-Shetland
76 Sill Complex (FSSC), with the central aim of investigating the distribution, timing and emplacement

77 of the FSSC and, in particular, to understand the regional magma flow network and main magma
78 input points into the FSB. Furthermore, given the prospective nature of the FSB, and the close
79 association of the FSSC with both source rocks and reservoir intervals, the potential impact of the
80 sill-network on the hydrocarbon system operating within the basin is investigated.

81 Although this study is focussed on the FSB, its findings have important ramifications for our
82 global understanding of the evolution and petroleum systems of other sedimentary basins and
83 rifted margins that have experienced considerable volcanism during their history (e.g. Brazil and
84 Africa – Gladchenko et al. 1997; Australia – Holford et al. 2012, 2013; China – Lee, 2006;
85 Greenland – Skogseid et al. 2000).

86

87 **Regional Geological History**

88 The FSB is the collective term for a series of rift basins situated between the Faroe Islands
89 and Shetland Isles that are affected by volcanism (Fig. 1), which are part of a much larger system of
90 rift basins that extends along the NE Atlantic Margin. The FSB experienced a complex multi-phase
91 rifting history, with several rift episodes occurring between the Permo-Triassic and Palaeocene,
92 culminating in breakup at 55 Ma (Ritchie et al. 2011). This was followed by Late Palaeocene and
93 Mid-Miocene basin inversion events (Smallwood and Maresh, 2002). The rift history has led to a
94 complex basin structure comprising a series of NE-SW trending “basement blocks”, consisting of
95 Precambrian crystalline igneous and metamorphic rocks, and incomplete occurrences of
96 Palaeozoic sedimentary rocks (e.g. Devonian). The blocks are capped with erosional remnants of
97 pre-rift Mesozoic sedimentary rocks, with adjacent fault bounded basins forming depocentres for
98 Cretaceous and Palaeocene sediments (Lamers and Carmichael 1999). The northeast Atlantic
99 region experienced considerable igneous activity prior to, and associated with, the onset of sea
100 floor spreading in the Late Palaeocene to Early Eocene (Fig. 2) (Passey and Hitchen, 2011; Ellis and
101 Stoker, 2014 and references therein). The earliest volcanism in the North Atlantic is thought to

102 have occurred ~63 Ma (Hamilton et al. 1998), before the onset of the eruption of the Faroe
103 Islands Basalt Group (FIBG) ~57 Ma (Passey and Jolley, 2009). Within the FSB, volcanism resulted
104 in the eruption of thick flood basalt sequences covering an area of at least 40,000 km². Despite
105 varying thicknesses of extrusive basaltic rocks within the various sub-basins forming the FSB, all
106 the basins contain a suite of intrusive mafic sills and dykes (Stoker et al. 1993, Gibb and Kanaris-
107 Sotiriou 1988; Thomson and Schofield, 2008; Schofield et al. 2012b), which are thought to have
108 been intruded between 55 and 53 Ma (Ritchie and Hitchen, 1996).

109 A series of 'transfer lineaments' are thought to transect the sub-basins in a NW-SE
110 direction (Rumph et al. 1993; Ellis et al. 2009; Ritchie et al. 2011), roughly perpendicular to the
111 dominant structural trend of the basin (Fig. 1). The lineaments within the FSB are thought to have
112 originated during the Phanerozoic/Palaeozoic and formed during the Caledonian Orogeny as deep
113 seated compressional transfer zones (Rumph et al. 1993; Ellis et al. 2009). Although the presence
114 and origin of the lineaments is uncertain (Moy and Imber, 2009), they are thought to have had
115 some control on sediment routing and provenance within the FSB, as well as controlling potential
116 sites of magma intrusion (Rumph et al. 1993; Jolley et al., 2005; Jolley and Morton, 2007; Ellis et al.
117 2009; Passey and Varming, 2010).

118 Various stratigraphic schemes have been applied to the FSB over the last 35 years. This
119 study uses the lithostratigraphy presented in Ritchie et al. (2011) and Stoker and Varming (2011),
120 which adopts the Palaeocene T-Sequence chronostratigraphy of Ebdon et al. (1995) (Fig. 2).

121

122 ***Palaeogene Volcanic History of the Faroe-Shetland Basin***

123 The FSSC has been estimated to cover a minimum area of at least 22,500 km², extending
124 from the Foinaven and Judd sub-basins in the SW of the FSB to the Møre Basin in the NE (Passey
125 and Hitchen, 2011). The true extent of this complex is likely to be much larger, as it extends
126 beneath the lava field(s) of the FSB (Passey and Hitchen, 2011). The sills as a whole form part of a

127 much more extensive series of Late Cretaceous/Palaeogene aged sill-complexes extending for
128 ~1800 km from the Norwegian Margin to the Southern Rockall Basin (Magee et al. 2014).

129 Limited radiometric dating of the FSSC has been undertaken, with the most reliable and
130 accepted dates clustering around 55-52 Ma (Passey and Hitchen, 2011), although sills as old as the
131 Campanian (72.1–83.6 Ma) have been reported (Fitch et al. 1988). The age clustering around 55-52
132 Ma extends from the Mid-Flett Formation (sequence T40/T45 boundary) through the Balder
133 Formation (sequence T50) and into the Middle to Early Eocene Horda Formation (Passey and
134 Hitchen, 2011).

135

136 **Methodology and Seismic Resolution**

137 *Data*

138 The main 3D seismic dataset used in this study is the Faroe–Shetland PGS MegaSurvey Plus, which
139 covers an area of ~24,000 km² (Fig. 1). The dataset is one of the largest regional seismic datasets
140 within the FSB, and has undergone substantial reprocessing to improve both sub-basalt and sub-
141 intrusive imaging within the basin, leading to considerable improvement in imaging of the FSSC.
142 This has been achieved via improved multiple attenuation, detailed velocity analysis, and utilisation
143 of improved migration techniques, leading to a greatly enhanced signal-to-noise ratio within the
144 data. As a result, there is substantial improvement in the quality of definition of deeper structural
145 elements of the basin, in particular the Base Cretaceous/Top Jurassic surface (Fig. 3).

146

147 *Sill Characterisation and Discerning Magma Flow from Seismic Data*

148 Sills imaged within 3D seismic datasets are typically identified by their tendency to crosscut
149 stratigraphy, their laterally discontinuous nature, and their high seismic amplitudes (Smallwood and
150 Maresh, 2002). Within a 3D seismic dataset, sill geometry can be constrained by manual picking
151 and volume visualisation techniques, such as opacity rendering. Opacity rendering techniques work

152 best when a seismic 3D dataset possesses large amplitude contrasts between different
153 stratigraphic sequences; this allows certain amplitudes to be selected in the volume and their
154 transparency manipulated (Kidd, 1999; Thomson and Schofield, 2008). This method is highly
155 effective for the examination of mafic sills intruded into sediments, as the sills exhibit higher
156 acoustic impedances than the surrounding country rock (Bell and Butcher 2002; Smallwood and
157 Maresh 2002; Planke et al. 2005). The result is a strong reflection coefficient at the boundary
158 between sediment and sill.

159 It has been demonstrated from several field and seismic studies that sills typically possess
160 lobate geometries, which are formed during magma intrusion and propagation (Thomson and
161 Hutton, 2004; Hansen and Cartwright, 2006; Schofield et al. 2012a). Opacity rendering has proven
162 particularly successful in enabling imaging of such magma lobes within the subsurface (see
163 Thomson, 2007; Schofield et al, 2012b), and by mapping these lobate geometries in 3D seismic
164 datasets, it is possible to interpret detailed magma flow pathways within sills (Fig. 4) (see Thomson
165 and Hutton, 2004; Hansen and Cartwright, 2006, Miles and Cartwright, 2010). Most previous
166 work has mapped magma flow pathways within individual sills or small sample populations in 3D
167 seismic datasets (e.g. Hansen and Cartwright, 2006; Schofield et al. 2012b). However, due to our
168 large regional dataset, we have been able to image and interpret the flow direction in ~100 sills
169 across the FSB in three dimensions, and in many cases, map flow directions back to origin/entry
170 points or zones within the basin (Fig. 5). Magma flow directions and entry points/zones are
171 discussed in detail below.

172

173 *Seismic Resolution*

174 When undertaking seismic interpretation of a basin containing intrusive and extrusive igneous
175 rock, it is critical to fully understand the changes (and reduction) in seismic resolution with depth,

176 especially as the attenuating effect intrusions have on seismic energy leads to rapid decreases in
177 frequency content with depth, decreasing the resolvability of deeper intrusions.

178 Within the FSB, this aspect is further compounded by the relatively large depth ranges
179 within the contemporary basin fill of the FSSC. For example, within the central Flett Basin, the sill
180 complex (e.g. Fig. 4) occurs at 3.5 sec TWT (equivalent to ~3 km below the sea-bed) and deeper.
181 At these levels, the dominant frequency of the seismic data is already significantly decreased via
182 normal attenuating effects of the overlying sedimentary overburden.

183 Quantifying how vertical seismic resolution decreases with depth is therefore essential in
184 understanding what thickness of intrusions can be imaged at different stratigraphic levels within the
185 FSB. Vertical seismic resolution is the minimum thickness that a geological unit (e.g. sand bed or an
186 intrusion) needs to be for it to be visible as a discrete event on seismic data. Below this thickness,
187 events can ideally still be detected as a reflector, but in reality may be rendered indistinguishable
188 against the overall reflectivity of surrounding strata and/or seismic noise; this is known as the
189 thickness of detectability.

190 Within the Palaeocene sedimentary sections of the central Flett Basin (~3.5 sec TWT), the
191 average dominant frequency of seismic reflection data is 17 Hz, decreasing to approximately 14 Hz
192 within the Cretaceous sections. Average velocity values for the Palaeocene from well data (Well
193 205/10-2b) are around 2819 m/s, giving a vertical seismic resolution of just over 40 m, and a
194 thickness of detectability of ~20 m. Within the Cretaceous sedimentary section, which contains
195 the majority of the identified intrusions, the velocity varies from 3048 m/s at the top Cretaceous
196 to 4572 m/s at the base. This velocity range gives a vertical resolution ranging from 54 m (26 m
197 detectability) at the top of the Cretaceous, to 81 m (40 m detectability) towards the base of the
198 Cretaceous.

199 This decrease in seismic resolution is problematic, as it means that even thick intrusions (>
200 40 m) are potentially unresolvable in the deeper (~3.5 seconds TWT and below) sections of the
201 data.

202

203 **Constraints on the FSSC from well data**

204 Although the vertical seismic resolution and limits of seismic detectability can be determined for
205 each intruded Palaeocene and Cretaceous sequence across the FSB, these calculations only
206 provide a broad indication of the thickness of intrusions that can be easily defined from the seismic
207 data. It does not provide any constraints of intrusions in the basin that may be *unresolved*, and what
208 total thickness of intruded material this may represent, potentially leading to a skewed and
209 incomplete view of the FSSC from seismic data.

210 Figure 6a represents an analysis of 19 wells within the FSB that have penetrated the FSSC.
211 The wells run approximately along the strike of the basin from NE to SW (Fig. 1). Two additional
212 wells that penetrated the sill complex were not included in this analysis because they also
213 penetrate buried volcanic complexes of the Palaeocene Erlend Volcano and Brendan Volcanic
214 Centre. These centres potentially represent areas of highly focussed localized magmatism within
215 the FSB, and therefore may be unrepresentative of magma intrusion of the FSSC as a whole. The
216 analysed wells penetrated a total of 149 separate intrusions, with a cumulative vertical thickness of
217 just under 2.4 km of igneous rock. It should be noted that it is unlikely, given the location and areal
218 spacing of the wells, that the same intrusions have been sampled twice by different wells.

219 The analysis provides several important results. Firstly, it is apparent that the distribution
220 of sill thicknesses is positively skewed, with 110 of 149 intrusions measured (73%) being <15 m in
221 thickness. This is far below the range of seismic resolution and detectability in most areas of the
222 seismic dataset. The total thickness of sills in the 0-15 m range is 562 m, which represents ~24% of
223 the total thickness of sill material penetrated by the wells.

224 Sills in the 0-40 m thickness range account for 132 of the 149 intrusions, or ~88% of all sills
225 penetrated, and for almost half of the total thickness of all sills penetrated (1152 m). Given the 40
226 m vertical seismic resolution, the well data implies that up to 88% of the total sills will therefore,
227 not be expressed as discrete reflections in seismic data. A detailed analysis of well 205/10-2b
228 provides a striking illustration of this discrepancy (Fig. 6b). Only two of the intrusions
229 (representing ~40% of the intruded material in this well) can be clearly interpreted in the seismic
230 data as sills (and are each actually composed of two closely spaced separate intrusions). The other
231 sills penetrated by the well are either not imaged, or form indistinguishable interference events.

232 It is important to note that this inability to clearly image all the intrusions is a function of
233 the geology, and not the seismic data used in this study, which arguably represents some of the
234 best re-processed legacy data available regionally within the FSB (see Fig. 3). The same issues
235 would apply to any and all seismic datasets that currently exist in this region and in other igneous-
236 affected basins (i.e., it is not dataset specific), and would be even more profound on older legacy
237 data which that has not undergone substantial reprocessing.

238

239 **Sill Geometry, Distribution and Interpretation of Magma Flow Pathways in the FSSC**

240 Although a large proportion of the smaller intrusions may be potentially unresolvable seismically
241 within the FSB, it is apparent from the regional seismic data that large intrusions (> 40 m in
242 thickness), can often be easily identified and mapped. This section will consider the overall
243 geometry and distribution of the FSSC (Figs. 7, 9 and 11), in addition to the main magma flow
244 pathways discerned from 3D mapping of sill morphology (Fig. 5). For clarity in description, the FSB
245 is split into five areas (northern Flett and Sissal Sub-basins, northern Foula Sub-Basin, central Flett
246 and Foula Sub-basins, southern Flett Sub-basin, Corona Ridge) (Fig. 1) on the basis of distinct
247 trends in sill emplacement and/or the nature of the sills (e.g. size and morphology).

248

250 The northern Flett and Sissal Sub-basins contain a heavily intruded Cretaceous section (Line A-A'
251 Fig. 1, Fig. 7), with the sills forming a complex, laterally and vertically stacked series of
252 interconnected sheets. The large number of intrusions within the Cretaceous makes seismic
253 definition of the underlying basin fill and structure (including Jurassic sequences) challenging. The
254 sills within the heavily intruded Cretaceous section represent a ~1.5-2 km thick section containing
255 vertically stacked intrusions, with individual sills showing a general decrease in diameter from tens
256 of kilometres in diameter in deeper parts of the Cretaceous (at a depth of 5.5 km in the
257 contemporary basin fill), to 1-3 km in diameter close to the presumed palaeo-landsurface at the
258 time of intrusion (now at a depth of ~4 km in the contemporary basin fill), as constrained by
259 penetration of sub-aerial lava flows by well 214/9-1 and penetration of the uppermost part of the
260 sub-aerial volcanic sequence by well 214/4-1 (Fig. 7). The sill complex is bounded to the southeast
261 by basement highs, and to the northwest by the segmented Corona Ridge (Fig. 1), which forms the
262 highs and half-graben structure of the Sissal Basin between wells 214/4-1 (the Tobermory Gas
263 Field discovery well) and well 214/9-1 (Fig. 7).

264 Flow directions identified in intrusions (e.g. from magma lobes) within the northern Flett
265 and Sissal Sub-basins indicate two distinct trends of sill emplacement. The first trend, seen within
266 the Sissal Basin, is characterised by sills that are fed *away* from the NE-SW trending bounding
267 Sissal Basin Fault, in a NW to SE direction, and which climb mainly strata-bound towards the
268 southerly segment of the Corona Ridge and the intra-basin high penetrated by well 214/9-1. The
269 second trend, within the northern Flett Sub basin, shows a *diverging* set of magma flow directions
270 that also climb towards the bounding highs (Fig. 7), namely the southerly Corona Ridge splay
271 (penetrated by 214/9-1) to the NW and the Rona Fault and Rona Ridge to the SE.

272 These observations suggest that within the Sissal Basin, magma appears to have been
273 inputted away from the Sissal Basin Fault, whereas within the northern Flett Sub basin, magma
274 input into the basin was generally from several zones running through the central axis of the basin.

275

276 *Northern Foula Sub-basin*

277 The northern Foula Sub-basin is characterised by a series of rotated fault blocks, buttressed
278 against the intra-basinal high drilled by well 208/21-1 (Line A-A' Fig. 1, Fig. 7). The morphology and
279 size of the intrusions within this part of the FSSC are markedly different from those within the
280 northern Flett Sub-basin. This part of the FSSC is characterised by a series of small (1-3 km in
281 diameter) saucer-shaped and half-saucer-shaped intrusions, which climb and cut through the
282 Cretaceous and Lower Palaeocene basin fill towards the intra-basin high penetrated by well
283 208/21-1 (Figs. 7 and 8). Importantly, well 208/21-1 penetrated a series of sub-aerial basalt lava
284 flows (with notable reddening and weathering profiles) interbedded with siltstones, between
285 1667–1811 m below the seabed. The sedimentary interbeds contain terrestrial pollen and spore
286 flora, and based on palynological and stratigraphical relationships, the age of these sub-aerial lavas
287 is, at the latest, sequence T36 (~58.4 Ma). This age pre-dates the main sequence T40-T45 (~56.1–
288 55 Ma) phase of volcanism, which manifested in the eruption of the Faroe Island Basalt Group
289 (Passey and Jolley, 2009; Schofield and Jolley, 2013) and suggests that this area of the basin acted as
290 one of the first foci for magmatism and volcanism during Kettle Member times (~58.4 Ma).

291

292 *Central Flett and Foula Sub-basins*

293 The overall spatial distribution of sills in this part of the FSB narrows and follows the main Flett
294 Sub-basin (Line B-B' Fig. 1, Fig. 9), which becomes confined between the Flett Ridge and Corona
295 Ridge. The two largest (~20 x 10 km in dimension), discrete, seismically definable intrusions within
296 the FSB occur here, having been intruded along the Cretaceous-Palaeocene boundary. Below this

297 depth, the Cretaceous is pervasively intruded, with the FSSC forming a series of vertically stacked
298 intrusions, particularly within the central part of the sub-basin. This series of intrusions terminates
299 downwards against the inferred base of the Cretaceous sequence at a depth of ~6 km beneath the
300 present day seabed. The heavily intruded nature of this part of the basin makes it difficult to
301 distinguish deeper pre- and syn-rift structure and stratigraphy (e.g. the Jurassic).

302 The magma flow directions interpreted from the sills in this region suggest a magma source
303 slightly off-centre from the basin axis (to the west), and running parallel to the strike of the Flett
304 Sub-basin (Figs. 5 and Fig. 9). The main area of magma input seems to be the south-easterly dipping
305 Flett Basin Fault (FBF) (Figs. 1, 5 and 9), which appears to have acted as the main controlling fault
306 defining the half-graben geometry of the Flett Sub-basin.

307 Towards the Corona Ridge (left side of Fig. 9), sills have interacted with and preferentially
308 intruded Cretaceous-age syn-rift faults, exploiting the edge of the tilted fault blocks to climb to
309 stratigraphically higher levels (Thomson, 2007). These interconnected intrusions can be traced
310 back in three dimensions to the magma input zone of the FBF, demonstrating over 25 km of lateral
311 and ~3 km of vertical magma movement away from the inferred entry point of magma into the
312 basin fill (Fig. 5).

313 The intrusions in the central Flett Sub-basin have also led to the formation of a prominent
314 forced fold (Figs. 9 and 10) above the intrusions (Moy and Imber, 2009), which has an amplitude of
315 ~180 m (not corrected for compaction). The formation of the fold caused doming of the overlying
316 Vaila and Lamba formations, above the central Flett Sub-basin. This has created a large double-
317 domal structure with near four-way dip closure, measuring approximately 18 × 40 km in areal
318 extent (Fig. 10). This forced fold structure is well illustrated by Moy and Imber (2009) using the
319 Kettle Tuff regional horizon (sequence T36; 58.4 Ma), which forms an easily definable seismic
320 reflector. The crest of the fold is, however, actually higher in the stratigraphy, as evidenced by

321 clear onlap onto the top surface of the forced fold, demonstrating that the fold had palaeo-
322 surface/seabed topographic expression by late Lamba Formation times (i.e., 56.1 Ma).

323 Another noteworthy occurrence in the central Flett Sub-basin is the presence of sediment
324 volcanoes (Fig. 10). Grove (2013) identified a sediment volcano (~6.5 km in diameter, penetrated
325 by well 214/28-1), which appears to have erupted sand-rich sediment (~13 km³, non-decompactd)
326 in a series of underwater sediment turbidites emanating from a central “vent”. These sediments
327 clearly onlap the forced fold (Figs. 9 and 10). Grove (2013) also stated that the mound was draped
328 by sequence T45 sediments; however, our re-interpretation of biostratigraphic data suggests that
329 the drape is actually equivalent to the base of sequence T40 (Base Flett), and that the sediment in
330 the vent is composed of reworked Lamba Formation (Fig. 10d).

331 Other inferred sediment volcanoes matching the characteristics of the one identified by
332 Grove (2013) and at the same stratigraphic level, are visible along the NW and NE flank of the
333 central Flett forced fold (Fig. 10e). This suggests that a basin-wide series of sediment eruptions
334 occurred at approximately the same time.

335

336 *Southern Flett Sub-basin*

337 The southern Flett Sub-basin (Line A-A' Fig. 1 and Fig 11) contains relatively few visible intrusions
338 within the Cretaceous section, in comparison to both the central and northern Flett sub-basins.
339 Consequently, and in contrast to many other parts of the basin, imaging of the Base
340 Cretaceous/Top Jurassic sequences is possible. The Base Cretaceous/Top Jurassic stratigraphy in
341 this area is characterised by a zone of heavily intruded, laterally continuous, generally strata-bound
342 intrusions, which occupy a series of small half-graben structures (Fig. 11). The potential significance
343 of a pervasively intruded Base Cretaceous section for the petroleum system in the basin is
344 discussed later.

345 As with the central Flett Sub-basin, the FBF appears to have acted as the controlling
346 influence on the magma input point into this part of the basin. Magma flow directions within the
347 sills appear to diverge away from the south easterly-dipping FBF in a predominantly west to east
348 direction.

349

350 *Corona Ridge (Rosebank Field)*

351 The Corona Ridge has undergone increased hydrocarbon exploration activity since 2004, when a
352 major oil and gas discovery (Rosebank Field) was made in the Palaeocene lava flows and intra-
353 volcanic sediments that directly overlie it (Schofield and Jolley, 2013) (Fig. 12). The Cretaceous
354 sequences immediately adjacent to and above the Corona Ridge (including the intra-volcanic
355 hosted Rosebank Field) have some of the lowest density of intrusions throughout the FSB. The
356 major saucer-shaped intrusions in this area climb in a SW- to NE direction from the Corona Basin
357 towards the Corona Ridge (Fig. 5). A roughly 27 m thick sill was penetrated by well 213/27-2, but
358 the Rosebank discovery well (213/27-1z), which also penetrated Jurassic sequences, did not
359 encounter any sub-volcanic intrusions around the Base Cretaceous unconformity, in contrast to
360 the central Flett Sub-basin where intrusions at this level appear common (Fig. 11)

361 The saucer-shaped intrusion penetrated by well 213/27-2 is isolated and is seemingly not
362 connected to any sub-horizontal sill complex in the surrounding area, which may have acted as its
363 magma source (Fig. 5). The isolated nature of the intrusion, atop the Corona Ridge, therefore
364 suggests that it was sourced sub-vertically (dyke-fed) through the Corona Ridge itself, possibly via
365 one of the ridge bounding faults.

366

367 **Magmatic Plumbing: Transport through Sedimentary Fill or Crystalline Basement?**

368 Our interpretations appear to show that the vast majority of intrusive sheet magmatism within the
369 FSB was focused through the sub-basins (i.e., sedimentary depocentres). However, some isolated

370 intrusions on both the Corona Ridge and the Rona Ridge occur without any apparent connection
371 to the sill complexes present within the sub-basins (Figs. 5 and 9). These isolated intrusions
372 suggest magma transited through or close to (perhaps constrained by ridge bounding faults?) the
373 crystalline basement of the basement ridges. The low number of intrusions, however, suggests that
374 any magmatic system that became established through the basement ridges during the Palaeogene
375 appears to have been relatively minor compared to other areas of the FSB.

376 The timing of the intrusions associated with the basement ridges is not easy to determine.
377 However, on the Corona Ridge, near to the southern extent of the Rosebank Field, a small conical
378 volcano (1 km in diameter), which fed a series of lava flows (Fig. 12b, c and d), indicates that a sub-
379 vertical magmatic system existed until at least sequence T45 (Flett Formation; 55.2 – 55.9 Ma)
380 (Schofield and Jolley, 2013) (Fig. 12).

381

382 **Discussion Part I – Magmatic Plumbing of the Faroe-Shetland Sill Complex**

383 ***Age and Phases of Sill Intrusion***

384 The exact ages and phases of sill intrusion into the FSB have long been debated and various
385 attempts at constraining the age of the sills from radiometric dating have been attempted, with a
386 general clustering of ages between 55 and 52 Ma (Pasey and Hitchen, 2011), representing Mid-
387 Flett (the sequence T40/T45 boundary) to Balder times (Fig. 2). This timing is generally accepted
388 as reliable (Smallwood and Harding, 2009; Pasey and Hitchen, 2011), and constrains FSSC
389 emplacement to after the first main phase of volcanism of the FIBG (Pasey and Jolley, 2009).
390 However, some of the stratigraphic relationships appear at odds with this interpretation.

391 On the Rona Ridge, well 208/21-1 penetrated sequence T36 (~58.4 Ma) Kettla Member
392 lava flows (Figs. 7 and 8). Critically, intrusions appear to connect to the base of these flows and
393 the palaeo-surface upon which they were emplaced (Fig. 8), suggesting a genetic connection
394 between the fissure systems that fed the sequence T36 lava flows and the underlying sills. This

395 connection suggests that the intrusions in the vicinity of this area of the Rona Ridge are equivalent
396 in age to the sequence T36 Kettle Member lava units (or 58.4 Ma) and therefore, related to an
397 earlier phase of volcanism in the basin.

398 The identification of forced folds and onlap by subsequent sediment packages onto palaeo-
399 seafloor/surfaces above sills has been shown in many basins to be an accurate method for
400 determining the relative ages of intrusions (e.g. Hansen and Cartwright, 2006; Magee et al. 2014).
401 As described earlier, evidence of forced folding can be seen within the central Flett Sub-basin,
402 above the two sills located along the basin axis (Figs. 9 and 10). Onlaps onto this forced fold
403 suggest that within the central Flett Sub-basin, palaeo-seafloor topography was in existence as a
404 result of at least one major phase of sill intrusion having occurred by at least Top Lamba
405 Formation times (~56.1 Ma).

406 Absolute ages of sills within the FSSC obtained via radiometric dating of sills are limited
407 within the FSB. However, well 207/01a-4z, drilled on the Rona Ridge, approximately 24 km NE of
408 the Clair Field, intersects a sill that has been dated at 52.4 ± 1.5 and 52.5 ± 1.5 Ma, with the age
409 regarded as 'reliable' (Fig. 13) (see Passey and Hitchen, 2011). This age would constrain the
410 emplacement of this sill to after the deposition of the Balder Formation (54.3 Ma). However,
411 above this particular intrusion a domal forced fold at the Top Cretaceous surface (Fig. 13), with
412 clear onlap of Lamba and Sullom/Vaila formation-aged sediments onto the fold, demonstrates that
413 by at least the lower Vaila Formation (61.6 Ma), the sill intrusion had occurred. Based on these
414 stratigraphic relationships this would place the age of the sill ~7 Myr earlier than the radiometric
415 age.

416 This discrepancy between stratigraphic relationships and radiometric age questions the
417 validity of the published radiometric date for this sill, and also other dates on the age of the FSSC.
418 Currently available dates, especially those based on K-Ar dating techniques, which can be
419 erroneous due to unquantified argon loss (Kelley, 2002), should now be treated with caution,

420 unless supported by other evidence (e.g. utilization of forced folds) or more robust dating
421 techniques (e.g., U-Pb dating of baddeleyite/zircon).

422 Given these discrepancies, we conclude that the FSSC was not simply emplaced between
423 Mid-Flett to Balder times (55.2 Ma – 54.3 Ma), as is often accepted based on published data
424 (Passey and Ritchie, 2011), and that several older phases of intrusion have occurred starting at
425 least through the Late Cretaceous/Sullom into early Vaila (pre-T10 - T28), through to Lamba
426 Formation and Flett Formation times (56.1 Ma – 55.2 Ma; T36 – T45).

427

428 ***The Intra-Lamba/Flett Sediment Eruption Event***

429 Within the central Flett Sub-basin, the material erupted from the sediment volcanoes onlaps the
430 forced fold in the centre of the basin (Fig. 10). However, the angle of onlap and downlap from the
431 vent material does not appear to change onto the forced fold (Fig. 10c and e). This lack of change
432 in angle of the onlaps and downlaps discounts any model of incremental growth of the forced fold
433 with sediment eruption, and suggests that the sediment volcano eruptive event actually post-dated
434 the formation of the forced fold and thus, presumably intrusion of the underlying sills (Fig. 9).
435 Importantly, the onlap and downlap of the erupted sediments onto the Top Lamba Formation
436 surface, followed by the subsequent onlap of the Base Flett Formation onto the top of the
437 sediment volcano suggests that the sediment vents in the Flett Basin are neither Lamba Formation
438 (sequence T38) or Flett Formation (sequence T40) in age, but instead represent an Intra-
439 Lamba/Flett sediment eruption event.

440 Chimneys beneath the sediment volcanoes extend downwards (as denoted by zones of
441 seismic noise) and coincide with the tips of the underlying sills, suggesting that the sills were the
442 origin of the fluids that mobilised the sediment, a mechanism previously invoked on the Norwegian
443 Margin for hydrothermal vents (Svensen et al. 2004). However, the timing discrepancy between
444 sill emplacement and sediment eruption implies that either a second phase of sill intrusion

445 occurred (after that which formed the forced fold), or that the fluids themselves are not directly
446 related to the sills, and are instead related to a basin wide overpressured fluid expulsion event, as
447 is often invoked in other sand injection/expulsion complexes (e.g., North Sea – Huuse et al. 2007;
448 California - Vigorito and Hurst, 2009). Although it is logical to invoke a second phase of sill
449 intrusion, it is unclear why the first phase of sill intrusion, which possessed enough magma volume
450 to dome the palaeo-seabed, did not trigger rapid heating and sand remobilization at the time.

451 It may therefore be the case that the coincidence of the potential origin or source of the
452 vents with sill tips is more a function of the sills acting as ‘baffles’ to fluid expulsion during a release
453 of overpressure from the Cretaceous rather than as a direct result of sill intrusion triggering
454 sediment fluidization (*sensu* Kokelaar, 1982; Schofield et al. 2010).

455 Overpressure in basins is thought to be largely caused by two mechanisms: disequilibrium
456 compaction and gas generation (Osborne and Swarbrick, 1997). We suggest that the first phase of
457 sill intrusion, which led to the forced folding, may therefore have created the correct geological
458 conditions to form effective side seals and low permeability barriers (Rateau et al. 2013). Fluid
459 expansion, due to gas generation by heating (e.g., Svensen et al. 2004) then occurred, leading to
460 overpressure formation. This overpressure was then released during the second phase of sill
461 intrusion by breaching of sedimentary seals, and fluid escape being baffled through the basin fill by
462 the intrusion network.

463

464 **Regional Magma Plumbing**

465 *Seismic Imaging of Intrusive Rocks - what are we missing?*

466 From our analysis of well data, it may be the case that up to 88% of total sill intrusions within the
467 sedimentary fill of the FSB are not imaged clearly in seismic reflection data (Figs. 6). The ability
468 therefore, of seismic studies (including this one) to fully capture the true characteristics of
469 magmatic plumbing systems in sedimentary basins must be questioned. Any studies in the FSB, or

470 other basins globally, in which volumetric deductions are made about the amount of magma
471 present within a basin that are derived solely from the interpretation of either 2D or 3D seismic
472 data, needs to be treated with caution, as such studies are likely to underestimate the total volume
473 of intruded igneous rock. In the FSB, the potentially large amount of seismically-unresolvable
474 intrusions within the Cretaceous, particularly within the Flett Sub-Basin, raises the possibility that
475 the thickness of the sedimentary component of the Cretaceous succession has been considerably
476 overestimated in previous studies. Instead, a large proportion of the current thickness (~2-2.5 km
477 in thickness parts) could be potentially composed of igneous material in the form of un-imaged sill
478 intrusions. This scenario has profound implications for basin modelling and sediment budget
479 calculations with the pre-sill intrusion Cretaceous sedimentary thickness being overestimated.
480 Despite this, through well analysis, at least some constraints on the upper limit of intrusion volume
481 can be applied to basins along the north-east Atlantic margin.

482 We are unable to constrain the role of unimaged vertical, dyke-like sources in transporting
483 magma through the sedimentary fill of the FSB. Studies of sill complexes in other Large Igneous
484 Provinces (e.g. Karoo-Ferrar), have demonstrated that dykes often form a volumetrically minor
485 component of the magma plumbing system within sedimentary basins (Muirhead et al. 2014). The
486 extensive imaged network of interconnected sills in the FSB that can be traced both horizontally
487 and sub-vertically (e.g. central Flett Sub-basin) and appear to represent significant pathways of
488 magma suggest that true dykes (i.e., those cutting vertically through the system) may play a
489 relatively minor role in magma movement through the FSB.

490

491 *Regional Magmatic Plumbing of the Faroe-Shetland Sill Complex (FSSC)*

492 Magma flow directions in the FSSC appear to show that magma input into the FSB is controlled
493 primarily by the heavily structured nature of the sub-basins, and the strong underlying NE-SW
494 basement trend. This control of the basin structure is not necessarily surprising, given the long-

495 lived tectonic nature of the basin and reactivation of major structures (Dore et al. 1997; Johnson
496 et al. 2005). In particular, the bounding faults of half-grabens, and their hanging walls, appear to be
497 critical in acting as sites for magma intrusion into the FSB (Fig. 5).

498 Within the Flett Sub-basin, the flow directions and general morphology of the sills
499 indicates that their axial feeders were located at the lowest part of the basin, and hence likely the
500 thinnest crust. This relationship suggests that magma input was focused in these regions during
501 sequence T40 (~56.1–55.2 Ma). Within the northern Flett Sub-basin, magma input appears to have
502 taken place across a broad zone (Figs. 5 and 7). Towards the central and southern Flett Sub-basins,
503 the half-graben bounding Flett Basin Fault appears to have been a major zone of magma input for
504 ~80 km along strike (Figs. 5, 7 and 9). Within the Sissal Sub-basin, which is bounded between the
505 northern and southern splay of the Corona Ridge, the half-graben bounding Sissal Basin Fault has
506 also acted as a major magma input zone along strike for ~40 km (Figs. 5 and 7).

507 The existence and origin of the rift-oblique lineaments thought to cut the FSB (see Fig. 1)
508 have been debated by many workers (Dore et al. 1997; Lamers and Carmichael 1999; Naylor et al.
509 1999; Rumph et al. 1993; Jørgensen 2006; Jolley and Morton 2007; Ellis et al. 2009; Passey and
510 Varming 2010), with the placement of the lineaments even changing between publications, as
511 noted by Moy (2010). Moy and Imber (2009) concluded that there was no definitive evidence that
512 the Victory, Clair and Judd lineaments imparted a significant structural or geomorphological
513 control on basin development during the Cenozoic. However, to the SW of the study area, in the
514 Rockall Basin, it has been suggested that lineaments have focused magmatism, in particular igneous
515 centres (Archer et al. 2005; Hole et al. 2015).

516 Regional mapping of sills and magma flow directions in the FSB adds some interesting
517 aspects to this lineament debate. Firstly, it is not overly apparent that the lineaments correspond
518 with zones of increased intrusion density throughout the basin. For example, within the southern
519 Flett Sub-basin, the relative intrusion density between the Corona Lineament and Grimur Kamban

520 Lineament actually appears to be lower than the rest of the basin. Furthermore, the axial feeding
521 zones for the sills within the Flett Sub-basin appear to cut across several different lineaments
522 without any major change in either the emplacement direction or nature of intrusions sourced
523 from these input zones, with most magma being interpreted to have been fed into the basin fill via
524 normal faults (Fig. 5).

525 It should be noted however, that some areas of magma input in the basin do appear to
526 coincide with the traces of lineaments. In particular, the SE trace of the Clair Lineament appears to
527 directly correspond with a suite of isolated sills intruded above the Rona Ridge (Fig. 5), away from
528 the main sites of magma intrusion into the basin. The magma feeding these sills must have either
529 transited sub-vertically through or adjacent to the ridge, as no intersection with other sill
530 complexes can be seen.

531 Fracture systems within crystalline basement are typically inherited from older structures
532 or tectonic grain (Dore et al. 1997), and often undergo reactivation, especially if a basin has
533 experienced a protracted rift history, such as the FSB (Lamers and Carmichael 1999). Evidence
534 from deep seismic reflection profiles indicates that, in some cases, lineaments such as the Westray
535 Lineament may connect to the Moho (England et al. 2005). Therefore, where the Clair Lineament
536 has intersected the Rona Ridge, the confluence of the deep seated fracture systems may have led
537 to the creation of a preferential, but still restricted, pathway of magma through or adjacent to the
538 Rona Ridge.

539

540 **Discussion Part 2 - Impacts of the Faroe-Shetland Sill Complex on the Petroleum** 541 **System of the FSB**

542 The FSB represents a highly important petroleum province within the UKCS and has significant
543 future implications towards the energy security of the UK, with the potential in-place
544 hydrocarbons in the Atlantic margin thought to be ~7.15 billion barrels of oil equivalent (Gray,

545 2013). The FSSC has a close spatial association with both the Jurassic source rocks and Jurassic-
546 Palaeocene reservoir intervals. It is therefore important to explore the potential impact and
547 interaction of the FSSC with the petroleum system of the FSB.

548

549 ***Implications for Hydrocarbon Migration***

550 Given the high density of intrusions within the Flett, Sissal, Foula and Guorun sub-basins, (Figs. 5,
551 7, 9 and 11), it seems conceivable that the intrusions may have interacted with the FSB petroleum
552 system. The exact effect of sill intrusions on hydrocarbon and fluid migration in the subsurface of
553 the FSB is still uncertain. It has been suggested that the intrusions may possess a dual role with
554 respect to hydrocarbon and fluid migration within the subsurface of the FSB (Rateau et al. 2013).
555 The intrusions (or the surrounding contact metamorphic zones) may create barriers and baffles to
556 fluid flow within the subsurface; however, some of the intrusions within the Flett Sub-basin may
557 have also acted as fractured conduits to migrating gas (and possibly other HC types) (Rateau et al.
558 2013). It is currently not possible to know which intrusions within the FSB acted as low
559 permeability barriers or fractured conduits (potentially compartmentalizing reservoir and source
560 rock intervals); however, both scenarios occurring are likely.

561 The close spatial relationship between intrusions and the Laggan and Tormore gas fields
562 atop the Flett Ridge is striking (see Rateau et al. 2013) (Fig. 14). Detailed examination of the
563 seismic data demonstrates that the Tormore Field, in particular, has a close relationship with the
564 underlying intrusions, with sill tips extending close to the down-dip extent of the Tormore
565 reservoir sandstone body (Fig. 15). Although the sill tips themselves are exploiting normal faults
566 within the Vaila Formation, which could itself offer a HC pathway (Scotchman, 2006), the Vaila
567 Formation sequences within the FSB are shale rich and composed of a series of hemipelagic muds
568 interbedded with marine sandstone bodies (Knox et al. 1997). They are therefore susceptible to
569 the formation of shale smears along fault planes (Lindsay et al. 1993). The addition of intrusive sills

570 may have acted as a fractured and preferential migration conduit through otherwise impermeable
571 Vaila Formation mudstones, raising the suggestion that Tormore could have been charged via
572 hydrocarbons migrating up through the fractured intrusion (Fig. 15d) (*sensu* Rateau et al. 2013).

573

574 ***Role of the FSSC in the generative potential of the Jurassic source rocks***

575 The increasing amount of hydrocarbon discoveries within the FSB (e.g., Rosebank, Tormore,
576 Laggan, Tornado) demonstrate that a viable petroleum system does exist, even in close association
577 with the intrusive sill network. Within the FSB, the Jurassic represents the main source rock
578 region (Scotchman et al., 1998); however, the Jurassic is generally poorly imaged across large areas
579 of the FSB due to the overlying sill complex within the Cretaceous. Therefore, assessing the
580 potential role of intrusions on the source kitchen of the Jurassic is difficult, especially as most well
581 penetrations of the Jurassic are restricted to structural highs, where intrusions are generally
582 absent or of low frequency. However, the most recent reprocessed seismic data appears to show
583 that the Lower Cretaceous/Uppermost Jurassic is heavily intruded (Figs. 11).

584 Given our interpretation that faults bounding the structural highs act as the main magma
585 pathways into the basin, it seems likely that at least some of the Jurassic source kitchen was in
586 close proximity to magma during the Palaeogene, and that some magma may have intruded into
587 the poorly imaged Jurassic sections. In such a situation, direct heating of the Jurassic sequences
588 may have led to over-maturation of the source rock. Furthermore, compartmentalisation of the
589 source rock by interconnected intrusions may hinder migration efficiency from the source kitchen,
590 as although some intrusions within the FSB are thought to act as fractured conduits, others appear
591 to have fractures filled by secondary minerals (see Rateau et al. 2013).

592 The notion that as much as 88% of the intruded material in the basin is not properly
593 imaged is significant because the effect of igneous intrusions on the petroleum systems and their
594 distribution and geometry has not traditionally been considered in basin modelling of the FSB (e.g.,

595 Scotchman et al. 2006). It is likely that within the FSB at least, the FSSC had some effect on the
596 maturity of source rock regions. Where seismic data quality is good, a laterally continuous and
597 heavily intruded zone, ~500-1000 m in thickness, sits directly above the top Jurassic (e.g., Fig. 5
598 and 11). The resolvability of intrusions at this depth, where vertical resolution is around 114 m,
599 would suggest that the section is dominated by either a series of >114 m thick intrusions, or a
600 series of smaller intrusions forming an interference effect. The potential heating impact on the
601 underlying source kitchen from the overlying, heavily intruded section is significant, and we suggest
602 it should be properly considered in future basin models of the FSB.

603 The highly intruded nature of the lowermost Cretaceous (and possibly uppermost
604 Jurassic?) within the FSB could have led to hydrocarbon migration issues, if the intrusions (or
605 surrounding contact metamorphic zones) are acting in a sealing capacity, by trapping
606 hydrocarbons, in particular oil phases, close to the source. This scenario would have resulted in
607 reduced migration efficiency and charge into reservoirs in the basin since the emplacement of the
608 FSSC in the Palaeocene.

609

610 **Conclusions**

611 This paper provides a comprehensive overview of the Faroe-Shetland Sill Complex in the
612 Faroe-Shetland Basin, and represents the first basin-wide study of a sub-volcanic plumbing system
613 in a hydrocarbon-producing basin. The study provides the first high-quality regional map of sub-
614 volcanic intrusions in the FSB. We suggest that magma enters the basin at localities related to key
615 structural features and is emplaced both vertically and laterally in a complex network of stacked
616 sheets, that are typically strata-bound and/or exploit sub-basin faults. Magma flow directions are
617 resolved from detailed mapping of magma flow lobes and their interaction with host strata. We
618 have identified a prominent NE-SW axial feeding zone to the sills in the FSB. This feeding zone
619 cuts across many NW-SE structural (“transfer”) lineaments, and suggests that these lineaments

620 may not exert as important a tectonic control on the basin as previously suggested. The seismic
621 data, however, do provide evidence of lateral movement of magma through the crust and
622 demonstrate that existing models of vertically stacked volcanic-magmatic systems are potentially
623 oversimplified.

624 Despite the very high quality seismic data used in this study, comparisons of resolvable
625 intrusions with well data indicate up to 88% of sills in the basin may not be identified (this figure
626 could be potentially greater on older datasets). Although many such intrusions may be small, their
627 combined volume represents a significant amount of magma. These volumes are considerably
628 underestimated in existing basin models and may have significant impact on the hydrocarbon
629 system of the basin.

630 We have also identified the important effect of intrusions on the petroleum system.
631 Intrusions may be closely linked to oil and gas fields and may act as potential pathways for
632 hydrocarbon migration (e.g., due to fractures). The pervasive emplacement of intrusions into
633 particular strata in a basin such as the FSB can, however, lead to compartmentalization of the
634 petroleum system and significantly inhibit hydrocarbon migration and extraction.

635 The study demonstrates the consequences of magma intrusion into sedimentary basins.
636 We have provided a comprehensive regional case study of magma movement in the shallow crust
637 and its clear implications for petroleum systems, and suggest that similar studies will enhance
638 future basin analyses and exploration.

639

640 **Acknowledgments**

641 We would like to extend our gratitude to the reviewers, Simon Kattenhorn and David Moy,
642 whose careful reviews and comments greatly improved the paper. The editor is also thanked for
643 clear guidance. This paper is dedicated to the memory of Dr Ken Thomson, who pioneered early
644 work looking at intrusions within the Faroe-Shetland Basin. PGS are thanked for the generous

645 donation of the FSB MegaSurveyPlus dataset, which made this study possible, and for permission
646 to publish this work. The Rosebank Joint Venture Project (Chevron North Sea Limited, OMV
647 (U.K.) Limited, and DONG EandP (UK) Limited) is thanked for making Figure 12 available. Spectral
648 decomposition was carried out using Foster Findlay Associates' (FFA) GeoTeric software. Seismic
649 Interpretation was undertaken using IHS Kingdom Software. NS would like to acknowledge
650 support and generous research funding for "Regional Emplacement of the Faroe-Shetland Sill
651 Complex" from STATOIL FÆRØYENE AS, Chevron North Sea limited, Hess Limited, DONG
652 E&P (U.K.) and OMV (U.K.) Limited. Richard Lamb, Steve Morse, Mike Keavney and David Iacopini
653 are thanked for discussions and suggestions.

654

655 **Conflict of Interest**

656 No conflict of interest declared

657

658

659 **References**

- 660 Archer, S.G., Bergman, S.C., Iliffe, J., Murphy, C.M. and Thornton, M., 2005, Palaeogene igneous
661 rocks reveal new insights into the geodynamic evolution and petroleum potential of the
662 Rockall Trough, NE Atlantic Margin. *Basin Research*, v.17, pp. 171-201.
- 663 Barr D, Savory K.E., Fowler S.R., Arman K. and McGarrity J.P. (2007). Pre-development fracture
664 modelling in the Clair Field, west of Shetland. In: Lonergan L., Jolly R., Rawnley K and
665 Sanderson D.J. (Eds), *Fractured Reservoirs*. Geol. Soc. Lond. Spec Pub. NO 270, pp 205-
666 226.
- 667 Bastow, I. D., G. W. Stuart, J.-M. Kendall, and C. J. Ebinger (2005), Upper-mantle seismic structure
668 in a region of incipient continental breakup: Northern Ethiopian rift, *Geophys. J. Int.*, 162,
669 479–493.
- 670 Bell, B.R. and Butcher, H., 2002, On the emplacement of sill complexes: evidence from the Faroe-
671 Shetland Basin, in Jolly, D.W. and Bell, B., eds., *The North Atlantic Igneous Province:*
672 *stratigraphy, tectonic, volcanic and magmatic processes.*: Geol Soc Lond. Spec Pub 197, p.
673 307-329.

674 Bond, CE., Lunn, RJ., Shipton, ZK. and Lunn, AD. (2012). 'What makes an expert effective at
675 interpreting seismic images?'. *Geology*, vol 40, no. 1, pp. 75-78., DOI: [10.1130/G32375.1](https://doi.org/10.1130/G32375.1)

676 Cartwright, J. and Hansen, D.M., 2006, Magma transport through the crust via interconnected sill
677 complexes: *Geology*, v. 34, p. 929-932.

678 Coffin, M.F. (Eds.), Large Igneous Provinces: Continental, Oceanic and Planetary. Geophysical
679 Monograph, vol. 100. American Geophysical Union, Washington, DC, pp. 45–93.

680 Davies, R., Bell, B.R., Cartwright, J.A., Shoulders, S., 2002, Three-dimensional seismic imaging of
681 Palaeogene dike-fed submarine volcanoes from the northeast Atlantic margin: *Geology*, v.
682 30, p. 223-226.

683 Dore, A.G., Lundin, E.R., Fichler, C. and Olesen, O. 1997. Patterns of basement structure and
684 reactivation along the NE Atlantic margin. *Journal of the Geological Society, London*, 154,
685 85–92.

686 Duddy, I.R., Green P.F., Hegarty, K.A., Bray R.J. and O'Brien, G.W. (1998). Dating and duration of
687 hot fluid flow events determined using AFTA[®] and vitrinite reflectance-based thermal
688 history reconstruction. In: Parnell, J. (ed) Dating and duration of fluid flow and fluid - rock
689 interaction. *Geological Society Special Publication 144*, 41-51.

690 Ebdon, C.C., Granger, P.J., Johnson, H.D., and Evans A.M., 1995. Early Tertiary evolution and
691 stratigraphy of the Faeroe-Shetland Basin: Implications for hydrocarbon prospectivity. In:
692 Scrutton R.A., et al. (eds) Sedimentation and palaeoceanography of the North Atlantic
693 region, *Geological Society of London, Special Publication 90*: 51-69

694 Ellis, D., Passey, S.R., Jolley, D.W. and Bell, B.R. 2009. Transfer zones: The application of new
695 geological information from the Faroe Islands applied to the offshore exploration of intra-
696 basalt and sub-basalt strata. In: Varming, T. and Ziska, H. (eds) *Faroe Islands Exploration
697 Conference: Proceedings of the 2nd Conference. Annales Societatis Scientiarum,
698 Færoensis, Supplementum, 50*, 174–204.

699 Ellis, D., & Stoker, M. S. (2014). The Faroe–Shetland Basin: a regional perspective from the
700 Paleocene to the present day and its relationship to the opening of the North Atlantic
701 Ocean. *Geological Society, London, Special Publications*, 397(1), 11-31

702 England, R.W., McBride, J.H. and Hobbs, R.W. 2005. The role of Mesozoic rifting
703 in the opening of the NE Atlantic: evidence from deep seismic profiling across the Faroe
704 Shetland Trough. *Journal of the Geological Society, London*, 162, 661–673.

705 Emeleus, C.H, and Bell, B.R., 2005, *British Regional Geology: the Palaeogene volcanic
706 districts of Scotland (Fourth edition)*. (British Geological Survey, Nottingham)

707 Field, L., Barnie, T., Blundy, J., Brooker, R.A., Keir, D., Lewi, E., and Saunders, K., 2012a, Integrated
708 field, satellite and petrological observations of the November 2010 eruption of Erta Ale:
709 Bulletin of Volcanology, doi:10.1007/s00445-012-0660-7 (in press).

710 Gibb F. and Kanaris-Sotiriou, R. 1988. The geochemistry and origin of the Faeroe–Shetland sill
711 complex. In: MORTON, A. C. and PARSON, L. M. (eds) Early Tertiary Volcanism and the
712 Opening of the NE Atlantic. Geological Society, London, Special Publications, 39, 241–252

713 Gladchenko, T. P., Hinz, K., Eldholm, O., Meyer, H., Neben, S., and Skogseid, J. (1997). South
714 Atlantic volcanic margins. *Journal of the Geological Society*, 154(3), 465-470.

715 Gray, J., Petroleum prospectivity of the principal sedimentary basins on the United Kingdom
716 Continental Shelf, Department of Energy and Climate Change, available online:
717 [https://www.gov.uk/government/uploads/system/uploads/attachment_data/file/367282/UKC](https://www.gov.uk/government/uploads/system/uploads/attachment_data/file/367282/UKC_S_offshore_2013.pdf)
718 [S_offshore_2013.pdf](https://www.gov.uk/government/uploads/system/uploads/attachment_data/file/367282/UKC_S_offshore_2013.pdf)

719 Grove, C. 2013: Submarine hydrothermal vent complexes in the Paleocene of the Faroe–Shetland
720 Basin: Insights from threedimensional seismic and petrographical data. *Geology*, 41, 71–74.
721

722 Grove, C. 2014. Direct and Indirect Effects of Flood Basalt Volcanism on Reservoir Quality
723 Sandstone. Doctoral thesis, Durham University.

724 Hansen, D.M. and Cartwright, J., 2006, The three-dimensional geometry and growth of
725 forced folds above saucer-shaped igneous sills: *Journal of Structural Geology*, v. 28, p.
726 1520-1535.

727 Hamilton, M. A., Pearson, D. G., Thompson, R. N., Kelley, S. P. and Emeleus, C. H. 1998. Rapid
728 eruption of Skye lavas inferred from precise U-Pb and Ar-Ar dating on the Rum and Cuillin
729 plutonic complexes. *Nature*, 394, 260-262.

730 Hartley, R.A., Roberts, G.G., White, N. and Richardson, C. 2011. Transient convective uplift of an
731 ancient buried landscape. *Nature Geoscience*, 4, 562-565.

732 Hildreth, W. and Fierstein, J. (2000). Katmai volcanic cluster and the great eruption of
733 1912. *Geological Society of America Bulletin* 112, 1594–1620

734 Hole, M.J., Millett, J.M., Rogers, N.W., Jolley, D.W., 2015. Rifting and mafic magmatism in the
735 Hebridean Basins

736 Holford, S.P., Green, P.F., Hillis, R.R., Underhill, J.R., Stoker, M.S. and Duddy, I.R. 2010. Multiple
737 post-Caledonian exhumation episodes across northwest Scotland revealed by apatite
738 fission track analysis. *Journal of the Geological Society*, London, 167, 675-694

739 Holford, S.P., Schofield, N., Macdonald, J.D., Duddy, I.R., Green, P.F. 2012. Seismic analysis of
740 igneous systems in sedimentary basins and their impacts on hydrocarbon prospectivity:
741 examples from the southern Australian margin. *The APPEA Journal*, 52, 229-252.

742 HOLFORD, S.P., SCHOFIELD, N., JACKSON, C. A.-L., MAGEE, C., GREEN, P.F. and DUDDY,
743 I.R. 2013. Impacts of igneous intrusions on source and reservoir potential in prospective
744 sedimentary basins along the western Australian continental margin. In KEEP, M. and
745 MOSS, S.J. (Eds), *The Sedimentary Basins of Western Australia IV*. Proceedings of the
746 Petroleum Exploration Society of Australia Symposium, Perth, WA, 2013.

747 Johnson, H., Ritchie, J.D., Hitchen, K., McInroy, D.B., Kimbell, G.S., 2005. Aspects of Cenozoic
748 deformational history of the northeast Faroe–Shetland Basin, Wyville–Thomson Ridge and
749 Hatton Bank areas. In: Doré, A.G., Vining, B. (Eds.), *Petroleum Geology: Northwest*
750 *Europe*. Proceedings of the Sixth Petroleum Geology Conference. Geological Society,
751 London, 933–1007.

752 Jackson, C, Schofield, N., and Golenkov., B (2013) – Geometry and Controls on the Development
753 of Igneous Sill-Related Forced Folds: A 2D seismic reflection case study from Offshore
754 Southern Australia, *Geological Society of America Bulletin*, doi: 10.1130/B30833.1

755 Jolley, D. W. and WHITHAM, A. 2004. A stratigraphical and palaeoenvironmental analysis of the
756 sub-basaltic Paleogene sediments of East Greenland. In: Programme and Abstracts
757 Palaeogene Stratigraphy, Tectonics and Petroleum Geology of North West Europe.
758 Abstracts volume, Geological Society of London.

759 Jolley, D.W., Morton, A.C. and Prince, I.P. 2005. Volcanogenic impact on phytogeography and
760 sediment dispersal patterns in the NE Atlantic. In: Dore´, A.G. and Vining, B.A. (eds)
761 *Petroleum Geology: NW Europe and Global Perspectives*, Proceedings of the 6th
762 *Petroleum Geology Conference*. Geological Society, London, 969–975.

763 Jolley, D.W. and Morton, A. 2007. Understanding basin sedimentary provenance: evidence from
764 allied phytogeographic and heavy mineral analysis of the Paleocene of the NE Atlantic.
765 *Journal of the Geological Society*, London, 164, 553–563.

766 Jolley, DW., Bell, BR., Williamson, IT. and Prince, I. (2009). 'Syn-eruption vegetation dynamics,
767 paleosurfaces and structural controls on lava field vegetation: An example from the
768 Palaeogene Staffa Formation, Mull Lava Field, Scotland'. *Review of Palaeobotany and*
769 *Palynology*, vol 153, no. 1-2, pp. 19-33.

770 Jolley, DW., Passey, SR., Hole, MJ. and Millett, JM. (2012). 'Large-scale magmatic pulses drive plant
771 ecosystem dynamics'. *Journal of the Geological Society*, vol 169, no. 6, pp. 703-711.

772 Jørgensen, O. 2006. The regional distribution of zeolites in the basalts of the Faroe Islands and the
773 significance of zeolites as palaeotemperature indicators. In: Chalmers, J.A. and Waagstein,
774 R. (eds). Scientific Results from the Deepened Lopra-I Borehole, Faroe Islands. Geological
775 Survey of Denmark and Greenland Bulletin, Copenhagen, 9, 123-156.

776 Kelley, S. (2002), K-Ar and Ar-Ar Dating, in Noble Gases in Geochemistry and Cosmochemistry,
777 Rev. Mineral. Geochem., vol. 47, edited by D. Porcelli, C. J. Ballentine, and R. Wieler, pp.
778 785–818, Mineral. Soc. of Am., Washington, D. C.

779 Kidd, G. D. 1999. Fundamentals of 3D seismic volume visualization. *The Leading Edge*, 18, 702–
780 709.

781

782 Knox, R. W. O., S. Holloway, G. A. Kirby, and H. E. Baily (1997), *Stratigraphic Nomenclature of the*
783 *UK North West Margin*, vol. 2, Early Paleogene Lithostratigraphy and Sequence
784 Stratigraphy, Br. Geol. Surv., Nottingham, U.K.

785 Kokelaar, B.P., 1982, Fluidization of wet sediments during the emplacement and cooling of
786 various igneous bodies. *Journal of the Geological Society, London*, v. 139, p.21-33

787 Lamers, E. and Carmichael, S.M.M. 1999. The Paleocene deepwater sandstone play west of
788 Shetland. In: Fleet, A.J. and Boldy, S.A.R. (eds) *Petroleum Geology of Northwest Europe:*
789 *Proceedings of the 5th conference.* The Geological Society, London. 645-659.

790 Larsen, L.M., Waagstein, R., Pedersen, A.K. and Storey, M. 1999. Trans-Atlantic correlation of the
791 Palaeogene volcanic successions in the Faeroe Islands and East Greenland. *Journal of the*
792 *Geological Society, London*, 156, 1081–1095.

793 Larsen, R. B. and Tegner, C. 2006. Pressure conditions for the solidification of the Skaergaard
794 intrusion: eruption of East Greenland flood basalts in less than 300,000 years. *Lithos* 92,
795 181 to 197.

796 Lawver, L.A. and Müller, R.D. 1994. The Iceland hotspot track. *Geology*, 22, 311–314.

797 Leat, P. T. (2008). On the long-distance transport of Ferrar magmas. *Geological Society, London,*
798 *Special Publications*, 302(1), 45-61.

799 Lee, G. H., Kwon, Y. I., Yoon, C. S., Kim, H. J., and Yoo, H. S. (2006). Igneous complexes in the
800 eastern Northern South Yellow Sea Basin and their implications for hydrocarbon
801 systems. *Marine and Petroleum Geology*, 23(6), 631-645.

802 Lindsay, N. G., F. C. Murphy, J. J. Walsh, and J. Watterson, 1993, Outcrop studies of shale smear
803 on fault surfaces: International Association of Sedimentologists Special Publication 15,
804 p. 113-123.

805 Moy, 2009, The architecture, growth and tectono-stratigraphic significance of rift-oblique
806 lineaments on the NE Atlantic Margin, PhD Thesis, Durham University.

807 Magee C, Hunt-Stewart E, Jackson CA-L, 2013a, Volcano growth mechanisms and the role of sub-
808 volcanic intrusions: Insights from 2D seismic reflection data, *Earth and Planetary Science*
809 *Letters*, Vol:373, ISSN:0012-821X, Pages:41-53

810 Magee C, Briggs F, Jackson CA-L, 2013b, Lithological controls on igneous intrusion-induced
811 ground deformation, *JOURNAL OF THE GEOLOGICAL SOCIETY*, Vol: 170, Pages: 853-
812 856, ISSN: 0016-7649

813 Magee C, Jackson CA-L, Schofield N, 2013c, The influence of normal fault geometry on igneous sill
814 emplacement and morphology, *GEOLOGY*, Vol: 41, Pages: 407-410, ISSN: 0091-7613

815 Magee C, Jackson CA-L, Schofield N, 2014, Diachronous sub-volcanic intrusion along deep-water
816 margins: insights from the Irish Rockall Basin, *BASIN RESEARCH*, Vol: 26, Pages: 85-105,
817 ISSN: 0950-091X

818 Mark, D.F., Green, P.F., Parnell, J., Kelley, S.P., Lee, M.R., and Sherlock, S.C., 2008a, Late Paleozoic
819 hydrocarbon migration through the Clair field, west of Shetland, UK Atlantic Margin:
820 *Geochimica et Cosmochimica Acta*, v. 72, p. 2510–2533, doi: 0.1016/j.gca.2007.11.037

821 Marsh, B. D. (2004). A magmatic mush column rosetta stone: the McMurdo Dry Valleys of
822 Antarctica. *Eos*, 85(47), 497-592

823 Miles, A., and Cartwright, J. (2010). Hybrid flow sills: a new mode of igneous sheet
824 intrusion. *Geology*, 38(4), 343-346.

825 Millett, J.M. 2014. Unpublished PhD thesis, University of Aberdeen.

826 Morton, A., Ellis, D, Fanning, M., Jolley, D., and Whitham, A. 2012, Heavy mineral constraints on
827 Palaeogene sand transport routes in the Faroe-Shetland Basin, in Varming, T. Ed.,
828 *Proceedings of the 3rd Faroe Islands Exploration Conference*

829 Moy, D.J. and Imber, J. 2009. A critical analysis of the structure and tectonic significance of rift-
830 oblique lineaments ('transfer zones') in the Mesozoic–Cenozoic succession of the Faeroe–
831 Shetland Basin, NE Atlantic margin. *Journal of the Geological Society*, London, 166, 1–14.

832 Naylor, P.H., Bell, B.R., Jolley, D.W., Durnall, P. and Fredstead, R. 1999. Palaeogene magmatism in
833 the Faeroe–Shetland Basin: influences on uplift history and sedimentation. In: Fleet, A.J. and
834 Boldy, S.A.R. (eds) *Petroleum Geology of Northwest Europe*, Proceedings of the 5th
835 Conference. Geological Society, London, 545–558.

836 Osborne, M.J. and Swarbrick, R.E., 1997. Mechanisms for generating overpressure in sedimentary
837 basins: A reevaluation. *AAPG Bulletin*, v.81, p.1023-1041.

- 838 Pankhurst, R. J., Riley, T. R., Fanning, C. M. and Kelley, S. R. (2000). Episodic silicic volcanism in
839 Patagonia and the Antarctic Peninsula: chronology of magmatism associated with the break-
840 up of Gondwana. *Journal of Petrology* 41, 605–625.
- 841 Passey, S. R. and Bell, B. R. 2007. Morphologies and emplacement mechanisms of the la2va flows of
842 the Faroe Islands Basalt Group, Faroe Islands, NE Atlantic Ocean. *Bulletin of Volcanology*
843 70, 139–56
- 844 Passey, S.R., and Jolley, D.W., 2009, A revised lithostratigraphic nomenclature for the Palaeogene
845 Faroe Islands Basalt Group, NE Atlantic Ocean: *Earth and Environmental Science*
846 *Transactions of the Royal Society of Edinburgh*, v. 99, p. 127-158.
- 847 Passey, S. and Hitchen, K. 2011. Cenozoic (igneous). In: Ritchie, J.D., Ziska, H., Johnson, H. and
848 Evans, D. (eds). *Geology of the Faroe-Shetland Basin and adjacent areas*. British Geological
849 Survey and Jarðfeingi Research Report, RR/11/01, 209-228.
- 850 Passey, S.R. and Varming, T. 2010. Surface interpolation within a continental flood basalt province:
851 An example from the Palaeogene Faroe Islands Basalt Group. *Journal of Structural Geology*,
852 32, 709-723.
- 853 Planke, S., Rasmussen, T., Rey, S.S. and Myklebust, R. 2005. Seismic characteristics and distribution
854 of volcanic intrusions and hydrothermal vent complexes in the Vøring and Møre Basins. In:
855 Dore´, A.G. and Vining, N. (eds) *Petroleum Geology: Northwest Europe and Global*
856 *Perspectives—Proceedings of the 6th Petroleum Conference*. Geological Society, London,
857 833–844.
- 858 Rateau, R., Schofield., N and Smith, M., 2013, The potential role of igneous intrusions on
859 hydrocarbon migration, West of Shetland. *Petroleum Geoscience* 19, 259-272
- 860 Ritchie, J. D. and Hitchen, K. 1996. Early Paleogene offshore igneous activity to the northwest of
861 the UK and its relationship to the North Atlantic igneous province. In: KNOX, R. B.,
862 CORFIELD, M. and DUNNAY, R. E. (eds) *Correlation of the Early Palaeogene in*
863 *NorthwestEurope*. Geological Society
- 864 Ritchie, J.D.; Ziska, H.; Johnson, H.; Evans, D., eds. 2011 *Geology of the Faroe-Shetland Basin and*
865 *adjacent areas*. Nottingham, UK, British Geological Survey, 317pp. (RR/11/001)
- 866 Rumph, B., Reaves, C.M., Orange, V.G., and Robinson, D.L., 1993. Structuring and transfer zones
867 in the Faroe Shetland Basin in a regional tectonic context, 999-1009 in *Petroleum geology*
868 *of northwest Europe*, proceedings of the 4th conference. Paerker, J R (editor). (London: the
869 Geological Society)

870 Skogseid, J., Planke, S., Faleide, J. I., Pedersen, T., Eldholm, O., and Neverdal, F. (2000). NE Atlantic
871 continental rifting and volcanic margin formation. *Geological Society, London, Special*
872 *Publications*, 167(1), 295-326.

873 Saunders, A.D., Fitton, J.G., Kerr, A.C., Norry, M.J., Kent, R.W., 1997. The North Atlantic Igneous
874 Province. In: Mahoney, J.J.,
875 Scotchman, I.C., Carr, A.D., and Parnell, J., 2006, Hydrocarbon generation modelling in a multiple
876 rifted and volcanic basin: A case study in the Foinaven Sub-basin, Faroe-Shetland Basin, UK
877 Atlantic margin: *Scottish Journal of Geology*, v. 42, no. 1, p. 1–19.

878 Schofield, Nick (2009) Linking sill morphology to emplacement mechanisms. Ph.D. thesis,
879 University of Birmingham.

880 Schofield, N., Brown D.J., Magee C., Stevenson CT., (2012a) Sill morphology and comparison of
881 brittle and non-brittle emplacement mechanisms, Geological Society of London, *Journal of*
882 *the Geological Society of London*, V.169, p127-141 (awarded Young Author of the Year
883 Award by Geolsoc. London)

884 Schofield, N., Heaton, L., Holford, S., Archer., S., Jackson., C., Jolley., D.W.,(2012b) - Seismic
885 imaging of 'Broken-Bridges': Linking seismic to outcrop-scale investigations of intrusive
886 magma lobes, *Journal of Geological Society*, V.169, p421-426

887 Schofield, N., and Jolley, D.W (2013) – Development of Intra-Basaltic Lava Field Drainage Systems
888 within the Faroe-Shetland Basin, *Petroleum Geoscience*, Vol. 19, pp. 259-272

889 Smallwood, J.R. and Harding, A. 2009. New seismic imaging methods, dating, intrusion style and
890 effects of sills: a drilled example from the Faroe-Shetland Basin. In: Varming, T. and Ziska,
891 H. (eds). *Faroe Islands Exploration Conference: Proceedings of the 2nd Conference.*
892 *Annales Societatis Scientiarum Færoensis*, Tórshavn, 50, 104-123

893 Smallwood, J.R., Towns, M.J. and White, R.S. 2001. The structure of the Faroe-Shetland Trough
894 from integrated deep seismic and potential field modelling. *Journal of the Geological*
895 *Society, London*, 158, 409-412.

896 Smallwood, J.R. and Maresh, J., 2002, The properties, morphology and distribution of igneous sills:
897 modelling, borehole data and 3D seismic data from the Faeroe-Shetland area. In: Jolley
898 DW, Bell BR (eds) *The North Atlantic Igneous Province: Stratigraphy, Tectonic, Volcanic*
899 *and Magmatic Processes. Geol Soc London Special Pub 197*, p. 271-306.

900 Smallwood, J.R., Prescott, D. and Kirk, W. 2004. Alternatives in Paleocene exploration west of
901 Shetland: a case study. *Scottish Journal of Geology*, 40, 131–143.

- 902 Stoker, M.S., Hitchen, K. and Graham, C. C. 1993. The Geology of the Hebrides and West
903 Shetland Shelves, and Adjacent Deep Water Areas. United Kingdom Offshore Regional
904 Report, British Geological Survey, London.
- 905 Svensen, H., S. Planke, A. Malthe-Sørensen, B. Jamtveit, R. Myklebust, T. R. Eidem, and S. S. Rey
906 (2004), Release of methane from a volcanic basin as a mechanism for initial Eocene global
907 warming, *Nature*, 429, 542–545.
- 908 Thomson, K. and Hutton, D., 2004, Geometry and growth of sill complexes: insights using
909 3D seismic from the North Rockall Trough: *Bulletin of Volcanology*, v. 66, p. 364-
910 375
- 911 Thomson, K., 2007, Determining magma flow in sills, dikes and laccoliths and their implications for
912 sill emplacement mechanisms. *Bulletin of Volcanology*, 70, p. 183-201
- 913 Thomson, K., Schofield, N., 2008, Lithological and structural controls on the emplacement and
914 morphology of sills in sedimentary basins, *Structure and Emplacement of High-Level
915 Magmatic Systems*, Geol. Soc. London, Special Publication, 302, p. 31-44.
- 916 Vigorito, M. and Hurst, A. (2010). 'Regional sand injectite architecture as a record of pore-
917 pressure evolution and sand redistribution in the shallow crust: insights from the Panoche
918 Giant Injection Complex, California'. *Journal of the Geological Society*, vol 167, no. 5, pp.
919 889-904. [ONLINE] DOI: 10.1144/0016-76492010-004
- 920 White, R.S., Smith, L.K., Roberts, A.W., Christie, P.A.F., Kuszniir, N.J., T.I. Team., (2008) Lower-
921 crustal intrusion on the North Atlantic continental margin *Nature*, 452 (2008), pp. 460–465
- 922 White, R. S., and D. McKenzie, Mantle plumes and flood basalts, *J. Geophys. Res.*, 100, 17,543–
923 17,585, 1995.
- 924 White, R. S., Drew, J., Martens, H. K., Key, A. J., Soosalu, H. and Jakobsdóttir, S. S. (2011).
925 Dynamics of dyke intrusion in the mid-crust of Iceland, *Earth and Planetary Science Letters*,
926 304, 300–312, doi: 10.1016/j.epsl.2011.02.038
- 927 Wright, T.J., and 12 others, 2012, Geophysical constraints on the dynamics of spreading centres
928 from rifting episodes on land: *Nature Geoscience*, v. 5, p. 242–250,
929 doi:10.1038/ngeo1428.
- 930 Wyllie, P. J., 1984. Constraints imposed by experimental petrology on possible and impossible
931 magma sources and products *Phil Trans R Soc. Lond.* A310, 439-56
- 932 Zellmer, G and Annen, C 2008, 'An introduction to magma dynamics'. in: C Annen, Zellmer , F G
933 (eds) *Dynamics of crustal magma transfer, storage and differentiation*. Geological Society,
934 London, pp. 1 - 13

935 **Figures:**

936

937 **Fig. 1 - A)** Main structural configuration of the Faroe-Shetland Basin. Note the predominant SW-
938 NE structural trend of the basin (from Ritchie et al. 2011), consisting of a series of intra-basinal
939 basement highs separating sub-basins. **B)** Approximate outline of the study area, with wells and
940 seismic lines referred to in the text indicated.

941

942 **Fig. 2 –** Palaeogene stratigraphy West of Shetland (modified from Schofield and Jolley, 2013), with
943 British Geological Survey lithostratigraphy (Ritchie et al. 2011) and BP T-sequence framework
944 (after Ebdon et al. 1995), and the stratigraphical position of the Faroe Island Basalt Group (FIBG)
945 (after Passey and Jolley 2009).

946

947 **Fig. 3 –** Comparison between seismic line from PGS FSB MegaSurvey data (**A**) against the same
948 seismic line from the re-processed PGS FSB MegaSurveyPlus data (**B**). Note the improvement in
949 signal to noise levels, reduction in multiples and increased definition of deeper Cretaceous and
950 Top Jurassic structure in the re-processed data. Data courtesy of PGS.

951

952 **Fig. 4 – A)** Opacity render showing Sills A and B within the seismic data. **B)** Enlargement of A
953 showing the detailed structure of the two sills. Note the ragged, lobate nature of the outer edge
954 of the sills. **C)** The interpretation of magma flow directions within sills A and B, based on the
955 lobate geometries examined in three dimensions, following the methodology of Thomson and
956 Hutton (2004), Hansen and Cartwright (2006) and Schofield et al. (2012b).

957

958 **Fig. 5 – A)** Map showing the flow directions interpreted in sills across the FSSC (see main text
959 and Fig. 4 for details), along with major basin structure (after Ritchie et al 2011). **B)** Map showing a
960 schematic representation of the main zones of magma input into the FSB based on interpreted
961 flow directions within the sills of the FSSC, overlain on the basin structure map (from Ritchie et al.
962 2011).

963

964 **Fig. 6 - A)** Histogram of 19 wells across the FSB, which collectively penetrated 149 separate sill
965 intrusions. It should be noted that most intrusions within the FSB intrude into the base Palaeocene
966 and throughout the Cretaceous sequences. At these depths in the basin, vertical seismic resolution
967 is at best ~40 m. From the sills penetrated by wells, 73% of all the intrusions are <15 m thick,
968 substantially below the vertical resolution of seismic data, and 88% are <40 m thick. Therefore,

969 within the FSB potentially up to 88% of the total sills are not being imaged clearly within seismic
970 data. **B)** Lower zone of sills penetrated by well 205/10-2b. From the synthetic seismic well-tie
971 generated using the wavelet extracted from the range in which the sills occur, only the two largest
972 intrusions (representing 40% of the total thickness of intrusions in this zone) are clearly imaged as
973 discrete seismic reflectors. Although the other intrusions (representing 60% of the total thickness
974 of intrusions in this zone) form interference effects, they are not discernable as discrete intrusions,
975 meaning that based on seismic alone, the majority of the total thickness of intruded material has
976 been missed. Data courtesy of PGS (FSB MegaSurveyPlus).

977

978 **Fig. 7** – NW-SE trending seismic line through the northern Flett and Sissal Sub-basins intersecting
979 key wells (Fig. 1, A-A'), with accompanying geo-seismic interpretation and sub-basin divisions
980 marked (data courtesy of PGS FSB MegaSurveyPlus). Within the Sissal Basin, the main input point
981 of magma into the basin fill appears to be the Sissal Basin Fault (see Fig. 1). Within the northern
982 Flett Sub-basin, the magma input points into the basin fill appear to occur over a broad ~40 km
983 zone located along the central axis of the sub-basin. Well 208/21-1 penetrated an intra-basinal high
984 and sequence T36 sub-aerial lava flows, suggesting that volcanism in this area predated the main
985 eruption of the Faroe-Island Basalt Group (see Fig. 2).

986

987 **Fig. 8 – A)** Opacity rendered image of sills underlying the sequence T36 sub-aerial lava flow
988 penetrated by well 208/21-1. **B)** The sills form a series of interconnected intrusions that climbed
989 and fed magma towards the intra-basinal high penetrated by 208/21-1, and came into close contact
990 with the base of the sequence T36 sub-aerial lava. The close spatial relationship of these intrusions
991 with the sub-aerial lava flow suggests that the intrusions in this area of the basin are also sequence
992 T36 in age. The lava flows themselves appear to have an origin from a paleo-high and flowed down
993 a paleo-slope basinward in a westerly direction. Data courtesy of PGS (FSB MegaSurveyPlus).

994

995 **Fig. 9** - NW-SE trending seismic line through the central Flett Sub-basin intersecting key wells
996 (Fig. 1, B-B'), with accompanying geo-seismic interpretation and sub-basin divisions marked (data
997 courtesy of PGS FSB MegaSurveyPlus). Within the central Flett Sub-basin, the main input point of
998 magma into the basin appears to be the Flett Basin Fault. Over 25 km of lateral and 3 km of
999 vertical magma movement is interpreted to have occurred through interconnected sills exploiting
1000 a series of tilted fault blocks (see Thomson and Schofield, 2008). A prominent forced fold has
1001 domed the Top Lamba surface Sediment volcanoes erupted sediment onto this surface and fold

1002 (Intra-Flett/Lamba event; see text and Fig. 10 for details). The Foula Sub-basin is relatively devoid
1003 of sill intrusions, but above the Rona Ridge isolated intrusions occur, from magma likely sourced
1004 through the basement high.

1005

1006 **Fig. 10 - A)** Top Lamba surface with closure of forced folds and location of sediment volcanoes
1007 marked. **B)** Oblique view showing sediment volcano onlapping onto the forced fold, and
1008 downlapping onto Top Lamba surface. Data courtesy of PGS (FSB MegaSurveyPlus) **C)**
1009 Enlargement of seismic line shown in Fig. 9 showing sediment volcano (as described by Grove,
1010 2013) within the central Flett Sub-basin. Note the onlaps onto the sill induced forced fold, and
1011 downlaps onto the Top Lamba surface, demonstrating that the forced fold had paleotopographic
1012 expression before the eruption of the sediment volcano. Base Flett position is marked. **D)**
1013 Stratigraphic palynology of section from well 214/28-1, which penetrated the sediment volcano
1014 and overlying sediments. The sediment volcano is composed of a series of recycled flora from
1015 sequence T36, suggesting that mobilized sand which fed the volcano was sourced from the Lower
1016 Lamba Formation; however, the zone of seismic disturbance (A), possibly representing the fluid
1017 pipe, extends towards the Base Cretaceous, suggesting that the fluids which mobilized the sands
1018 may have been sourced from a deeper basinal level. **E)** Enlargement of another sediment volcano
1019 situated on the NW flank of the forced fold (Fig. 9). This sediment volcano sits at the same
1020 stratigraphic level as the one described by Grove (2013). Data courtesy of PGS (FSB
1021 MegaSurveyPlus)

1022

1023 **Fig. 11 -** NW-SE trending seismic line through the southern Flett Sub-basin intersecting key wells
1024 (Fig. 1, C-C'), with accompanying geo-seismic interpretation and sub-basin divisions marked (data
1025 courtesy of PGS FSB MegaSurveyPlus). Magma input into the southern Flett Sub-basin continues to
1026 be dominated by the Flett Basin Fault. Compared to other areas of the Flett Sub-basin, the
1027 southern Flett Sub-basin contains a lower frequency of intrusions, allowing for imaging of the base
1028 Cretaceous unconformity, which appears to be heavily intruded by a series of generally strata-
1029 bound intrusions that may cause a significant risk of igneous compartmentalization of the Jurassic
1030 source rocks.

1031

1032 **Fig. 12 –** Data courtesy of the Rosebank Joint Venture Project. **A)** Sequence T45 upper volcanics
1033 TWT surface map of the Rosebank Field located above the Corona Ridge. **B)** Seismic line through
1034 a 2 km wide volcanic edifice. **C)** Oblique view of the volcanic edifice, showing the central crater.

1035 **D)** Spectral decomposition conducted on the upper volcanic surface displayed as a RGB Blend (R=
1036 11 Hz, G=12 Hz, B = 13 Hz), which differentiates the lava field morphology, and illustrates that the
1037 volcanic edifice has fed a series of SE-flowing lava flows. This series of upper Flett, sequence T45
1038 lava flows illustrates that the Corona Ridge had undergone volcanism during these times.

1039

1040 **Fig. 13- A)** Seismic line tying well 214/30A-2 (Glenlivet Field) and well 207/01a-4z, which
1041 intersected a 146 m thick sill that was dated radiometrically at ~52.4 Ma, constraining its
1042 emplacement to post-deposition of the Balder Formation. The sill created a forced fold above the
1043 intrusion, which domed the Upper Cretaceous surface. Subsequent onlaps of the Lamba and Vaila
1044 sequences suggest that the forced fold had topography by Vaila times (63 – 58 Ma). Therefore, the
1045 underlying intrusion, which caused the forced fold, must pre-date the radiometric age by some 10
1046 to 5 Ma years, questioning the validity of the radiometric dating. **B)** Map of the Upper Cretaceous
1047 horizon in the vicinity of well 207/01a-4z showing the forced fold. **C)** Oblique view of the forced
1048 fold developed on the Upper Cretaceous horizon, and underlying sill intrusion. All data courtesy
1049 of PGS (FSB MegaSurveyPlus).

1050

1051 **Fig. 14 - A)** Opacity rendered image showing the sills within the central Flett Sub-basin, and the
1052 relative position of the Laggan and Tormore oil/gas fields. **B)** Enlargement of the Tormore oil/gas
1053 field showing the underlying sill complex. See Fig. 16 for detailed relationship. All data courtesy of
1054 PGS (FSB MegaSurveyPlus).

1055

1056 **Fig. 15- A)** Seismic line through the central Flett Sub-basin showing a sill in close association with
1057 the Tormore oil and gas field (205/5a-1) (Fig. 1, D-D'). **B)** Geo-seismic interpretation showing how
1058 the edge of the sill tips climb faults and extend close to the down-dip extent of the
1059 Laggan/Tormore Vaila-aged sand body. **C)** Enlargement of seismic line showing how the sill tip has
1060 climbed sub-vertically and extends close to down-dip extent of the Tormore sand body. Note the
1061 amplitude anomaly within the down-dip sand body located directly above the sill tip. **D)** Rotated
1062 phase (90°) envelope image illustrating the high amplitudes of the sill and Tormore gas leg. The sill
1063 tip can be seen within the fault plane, suggesting that hydrocarbon migration has taken place
1064 through the fractured sill into the Tormore Field. All data courtesy of PGS (FSB MegaSurveyPlus).

1065

1066

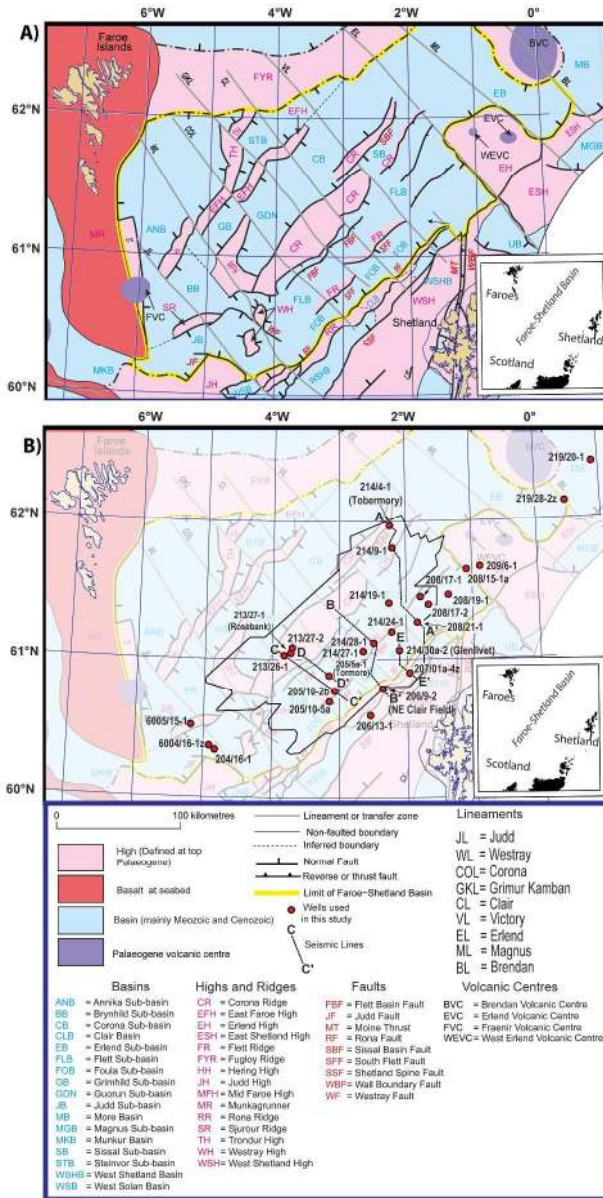


Fig 1
207x404mm (300 x 300 DPI)

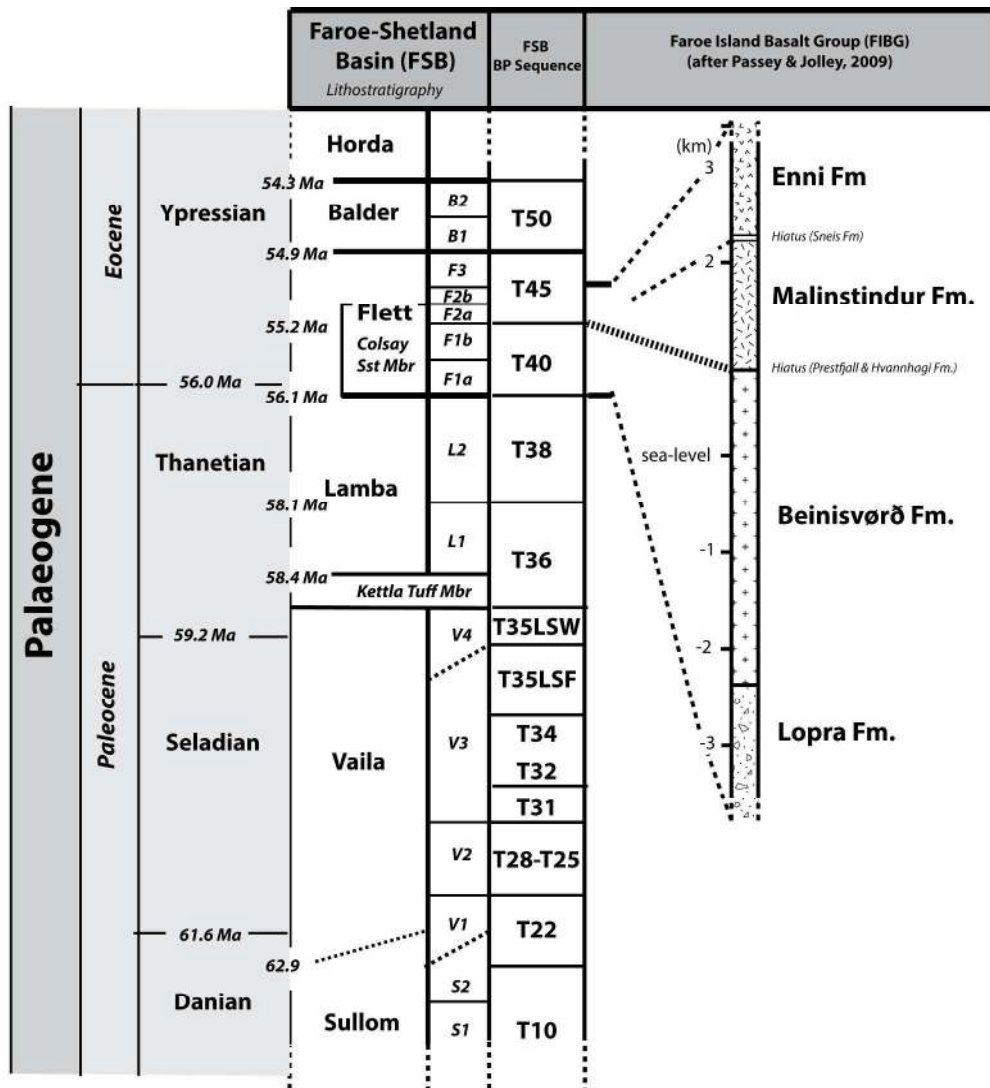


Fig 2
274x297mm (300 x 300 DPI)

1
2
3
4
5
6
7
8
9
10
11
12
13
14
15
16
17
18
19
20
21
22
23
24
25
26
27
28
29
30
31
32
33
34
35
36
37
38
39
40
41
42
43
44
45
46
47
48
49
50
51
52
53
54
55
56
57
58
59
60

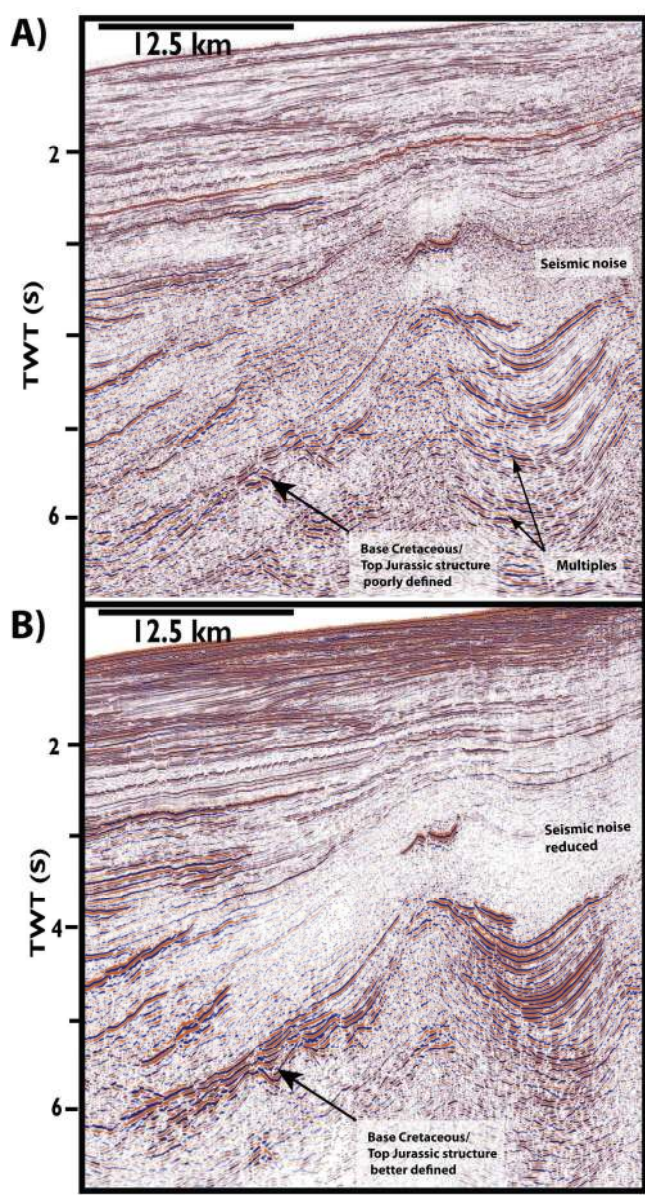


Fig 3
127x234mm (300 x 300 DPI)

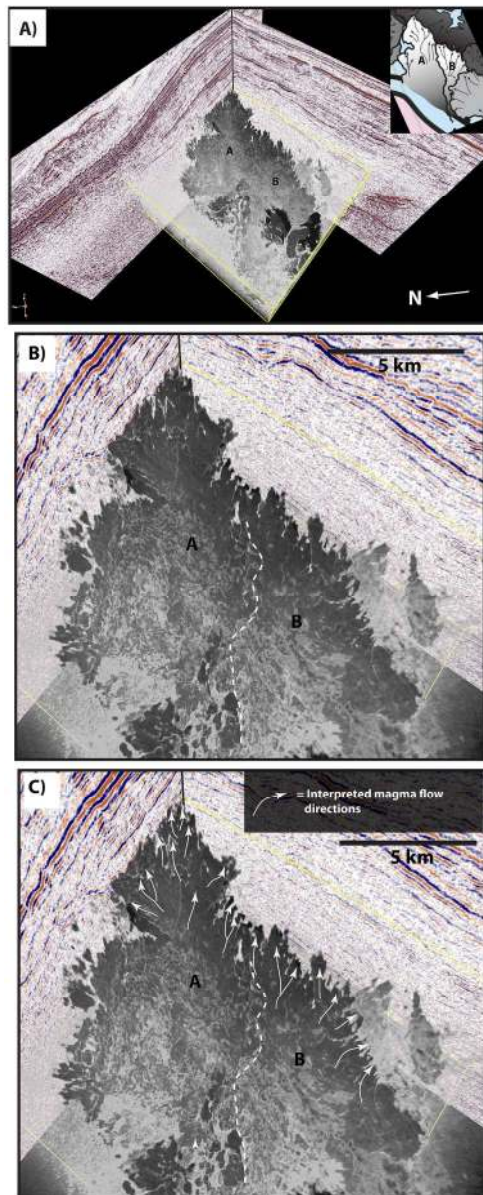


Fig 4
101x245mm (300 x 300 DPI)

1
2
3
4
5
6
7
8
9
10
11
12
13
14
15
16
17
18
19
20
21
22
23
24
25
26
27
28
29
30
31
32
33
34
35
36
37
38
39
40
41
42
43
44
45
46
47
48
49
50
51
52
53
54
55
56
57
58
59
60

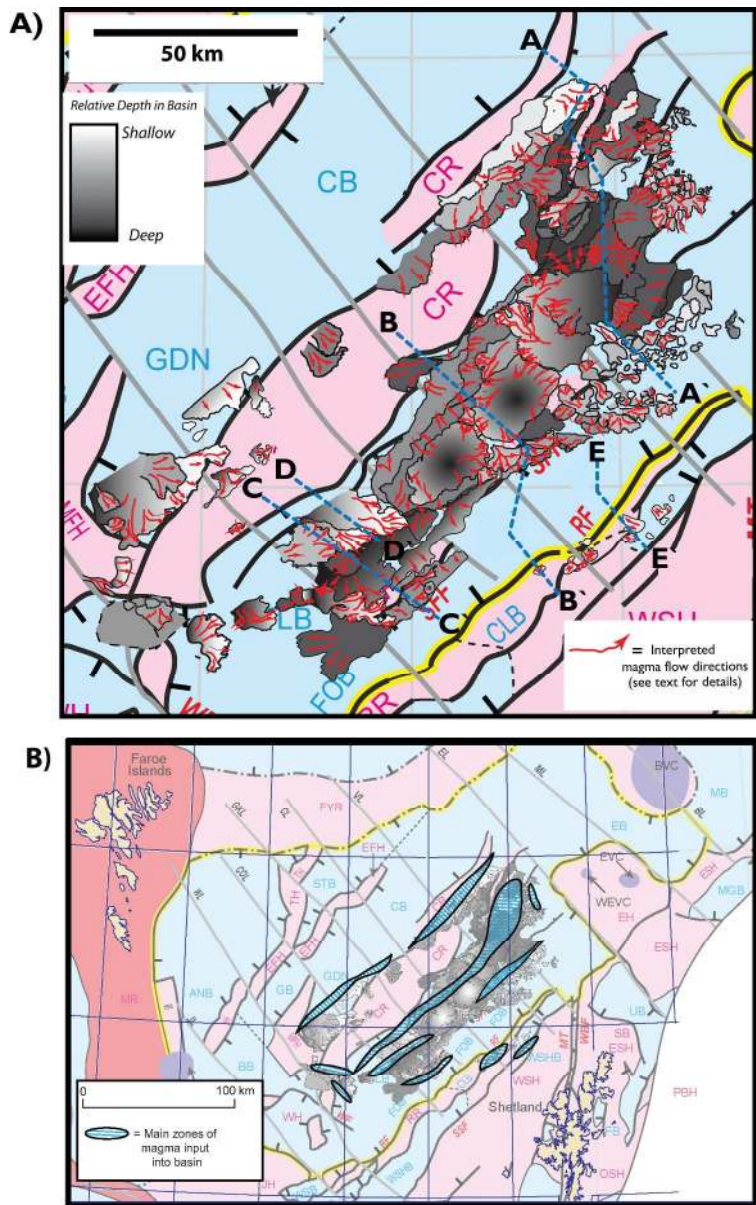


Fig 5
216x348mm (300 x 300 DPI)

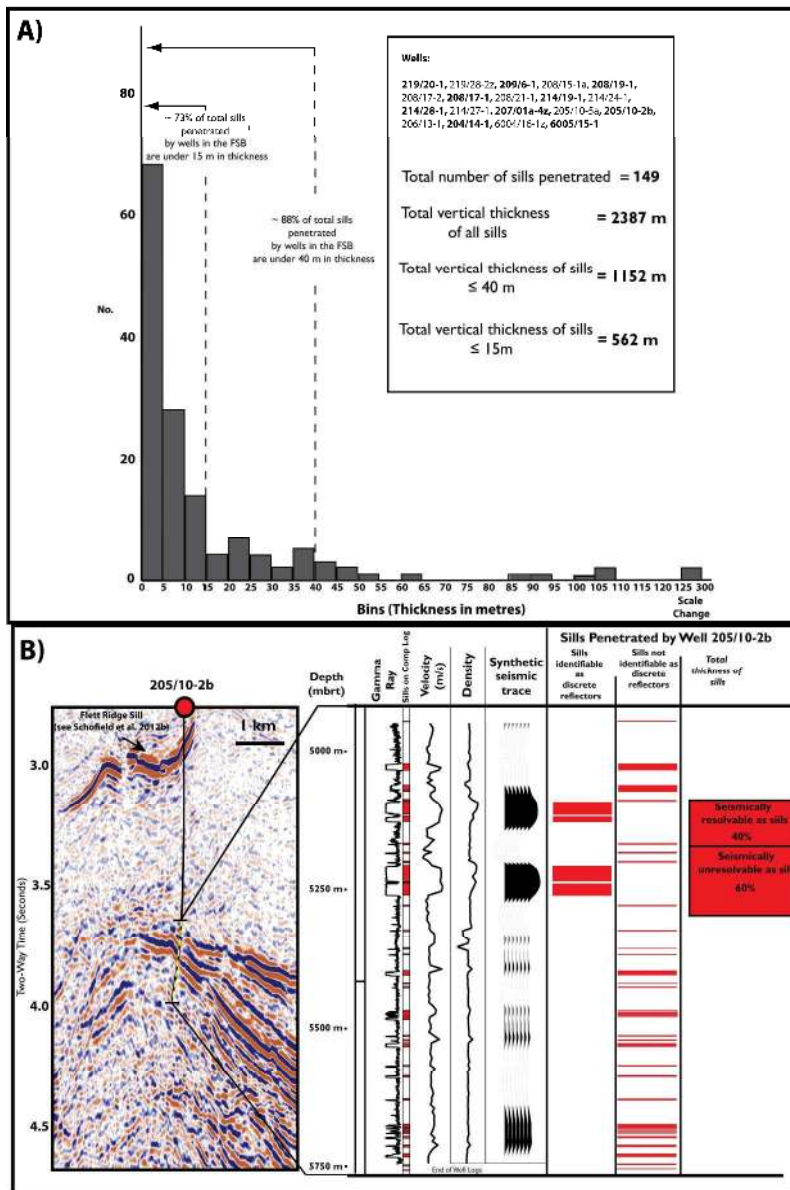


Fig 6
 211x318mm (300 x 300 DPI)

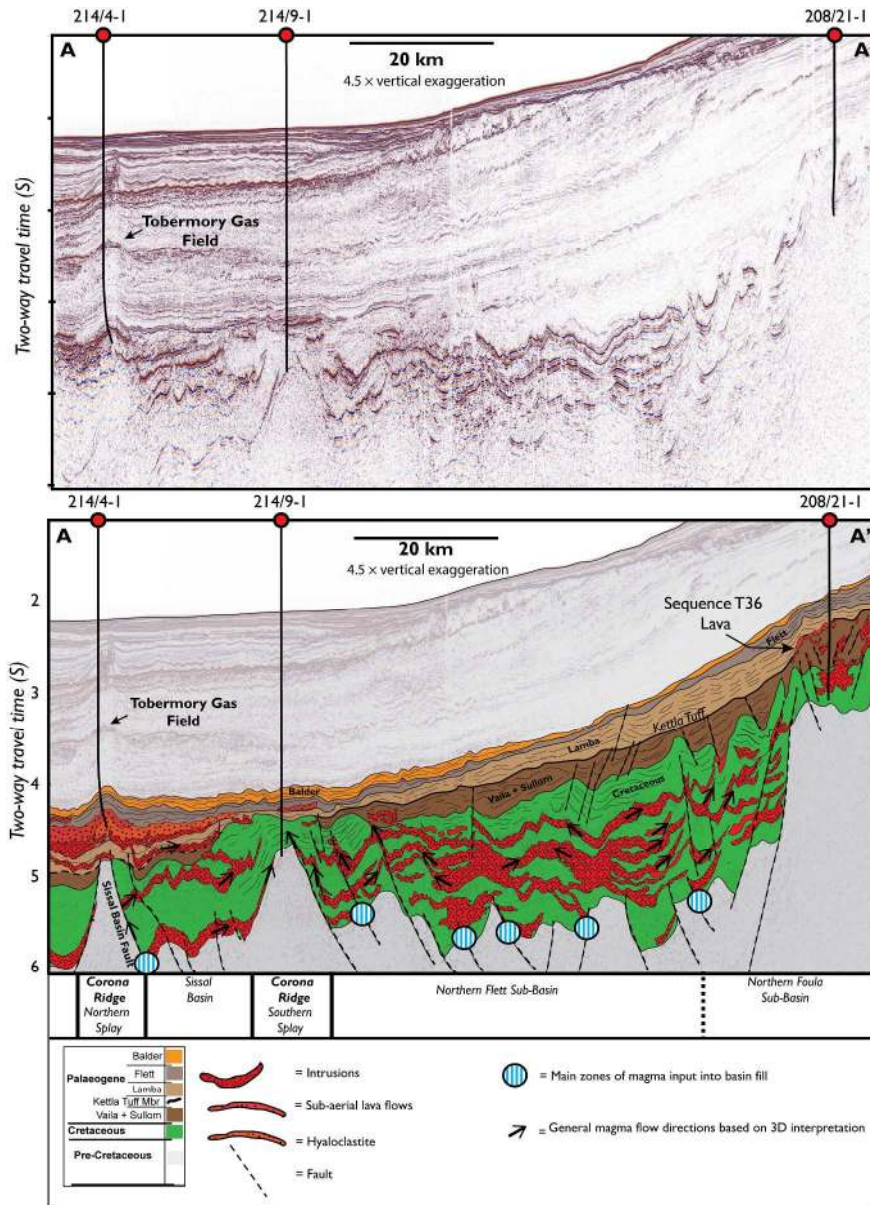


Fig 7
211x288mm (300 x 300 DPI)

1
2
3
4
5
6
7
8
9
10
11
12
13
14
15
16
17
18
19
20
21
22
23
24
25
26
27
28
29
30
31
32
33
34
35
36
37
38
39
40
41
42
43
44
45
46
47
48
49
50
51
52
53
54
55
56
57
58
59
60

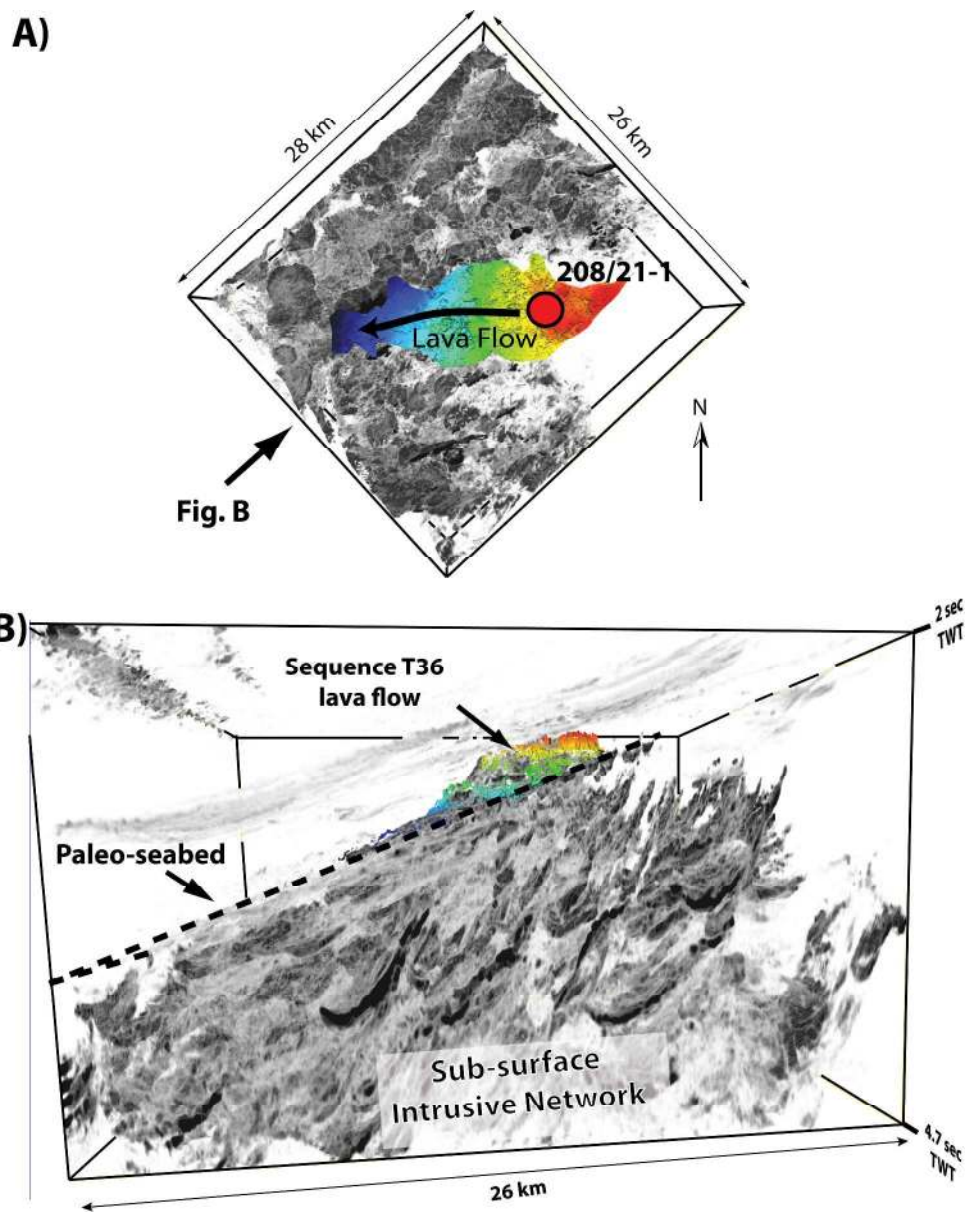


Fig 8
278x344mm (300 x 300 DPI)

1
2
3
4
5
6
7
8
9
10
11
12
13
14
15
16
17
18
19
20
21
22
23
24
25
26
27
28
29
30
31
32
33
34
35
36
37
38
39
40
41
42
43
44
45
46
47
48
49
50
51
52
53
54
55
56
57
58
59
60

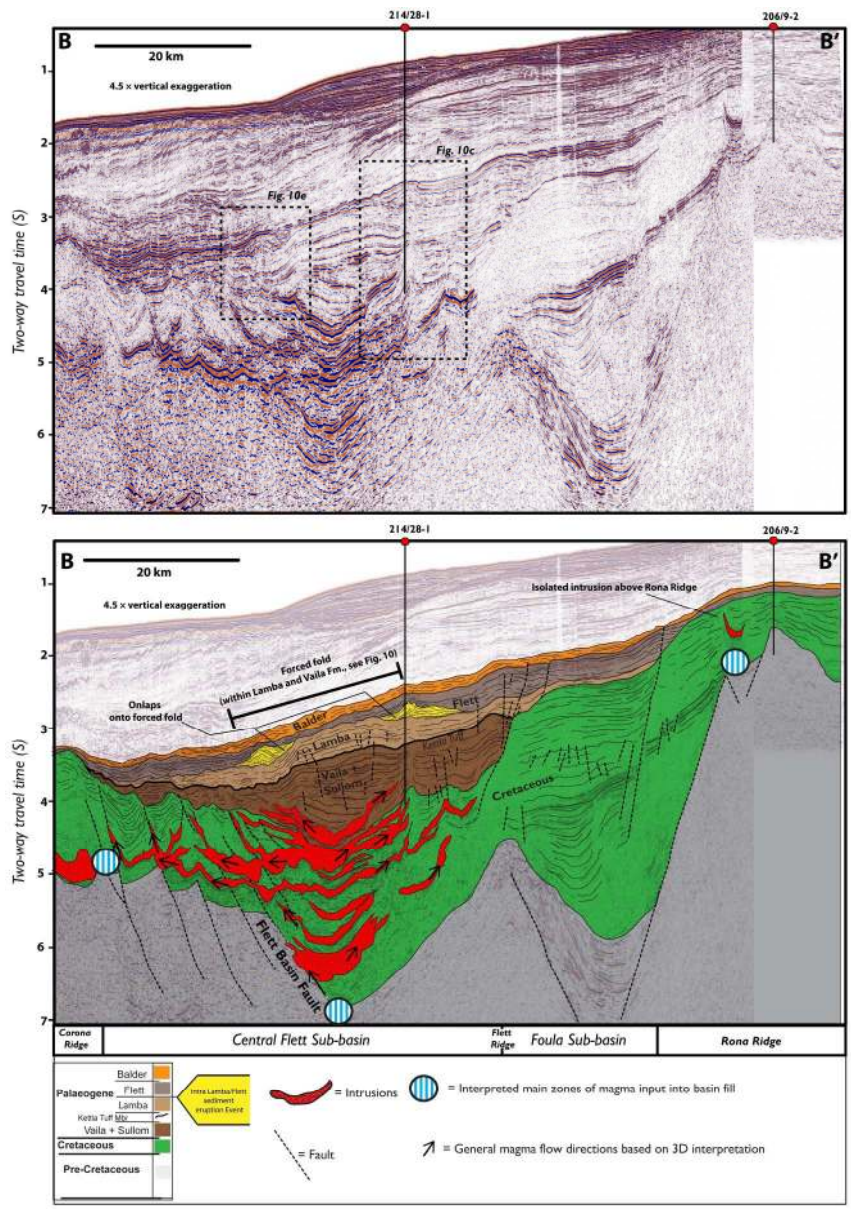


Fig 9
338x474mm (150 x 150 DPI)

1
2
3
4
5
6
7
8
9
10
11
12
13
14
15
16
17
18
19
20
21
22
23
24
25
26
27
28
29
30
31
32
33
34
35
36
37
38
39
40
41
42
43
44
45
46
47
48
49
50
51
52
53
54
55
56
57
58
59
60

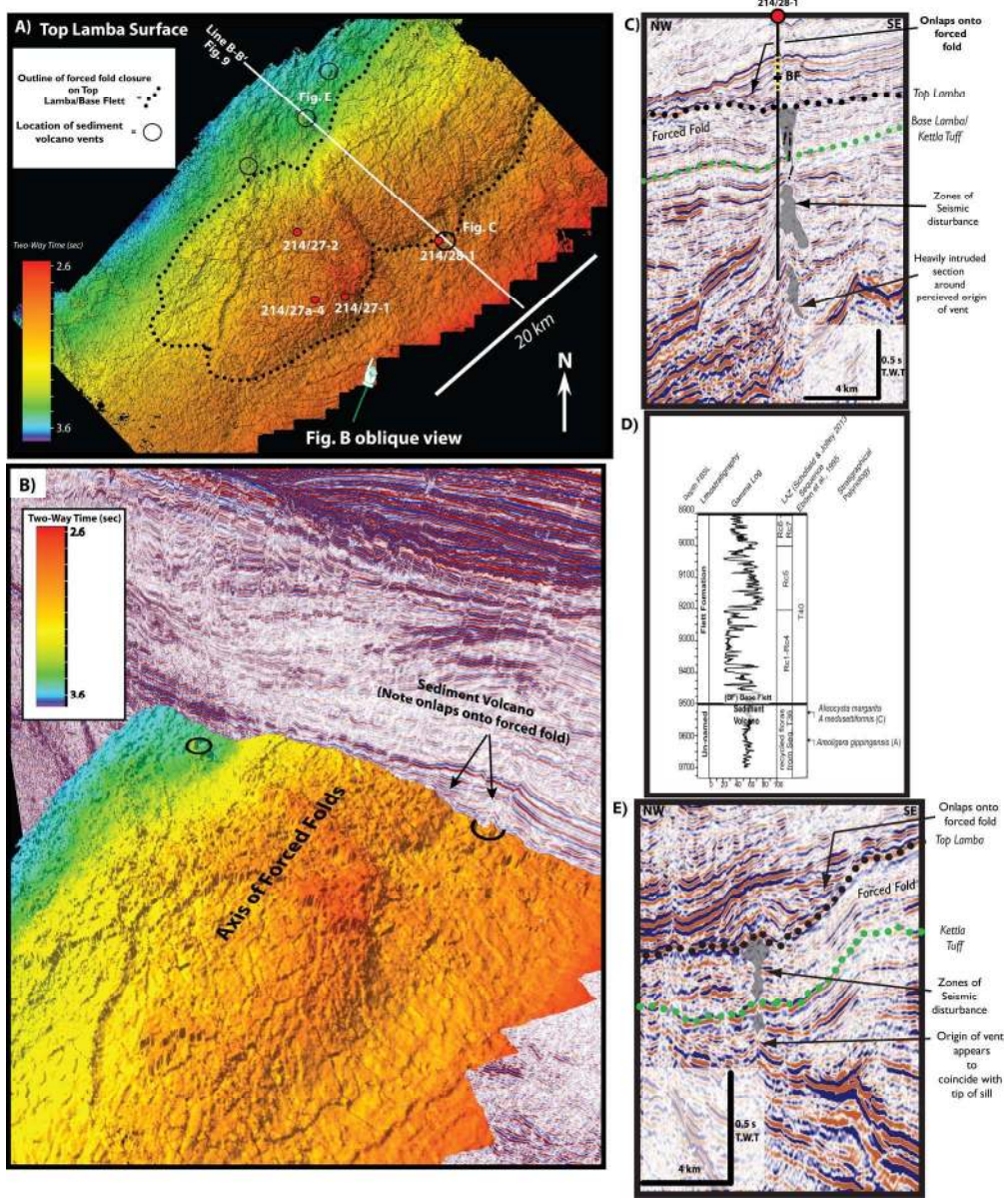


Fig 10
211x253mm (300 x 300 DPI)

1
2
3
4
5
6
7
8
9
10
11
12
13
14
15
16
17
18
19
20
21
22
23
24
25
26
27
28
29
30
31
32
33
34
35
36
37
38
39
40
41
42
43
44
45
46
47
48
49
50
51
52
53
54
55
56
57
58
59
60

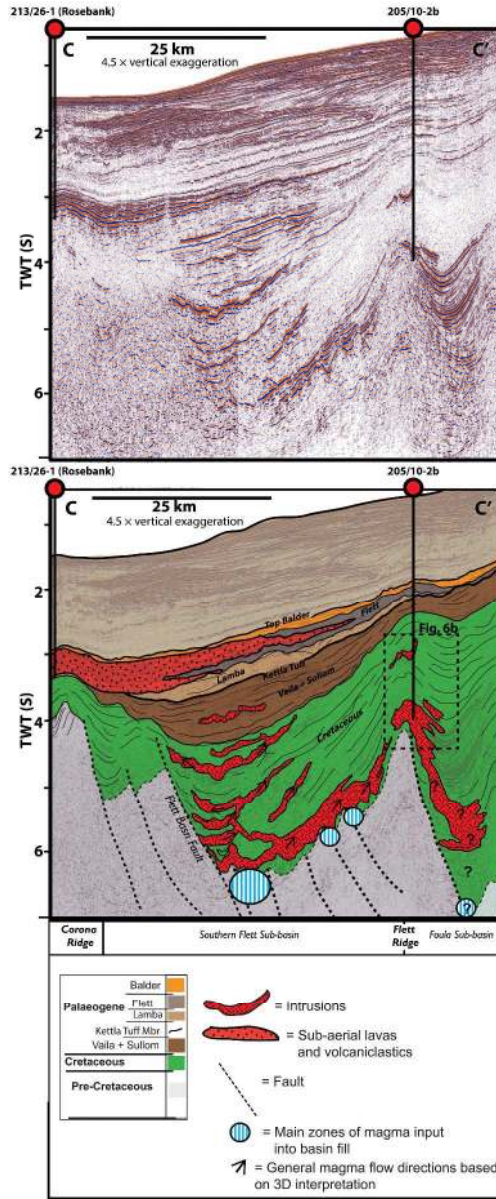


Fig 11
169x407mm (300 x 300 DPI)

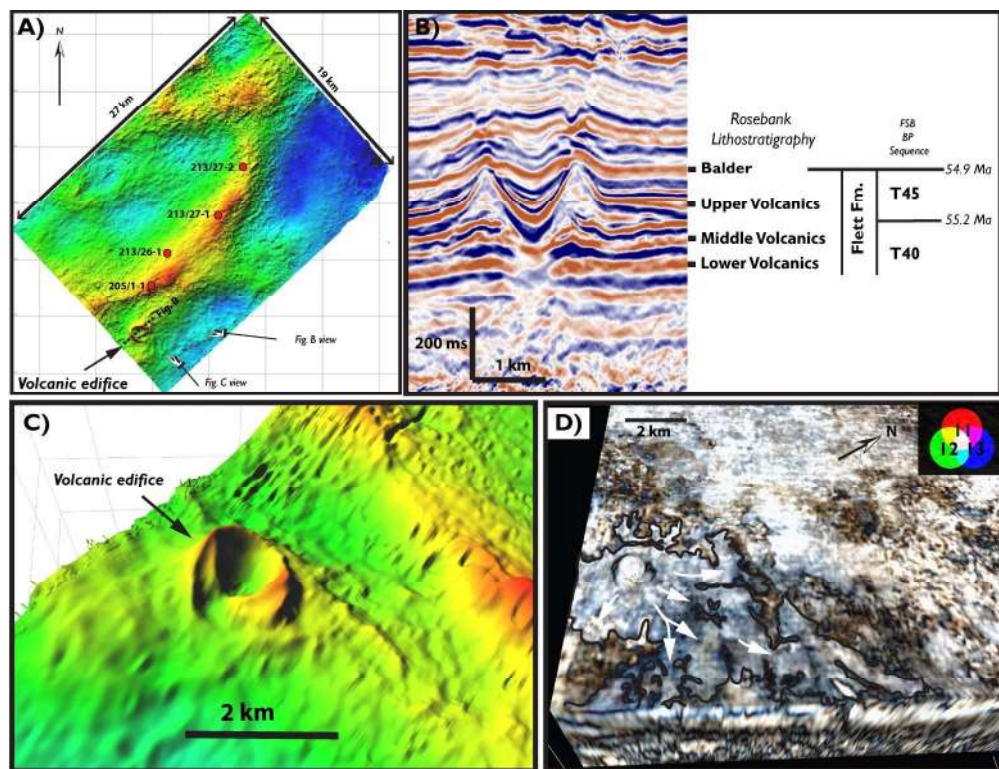


Fig 12
211x161mm (300 x 300 DPI)

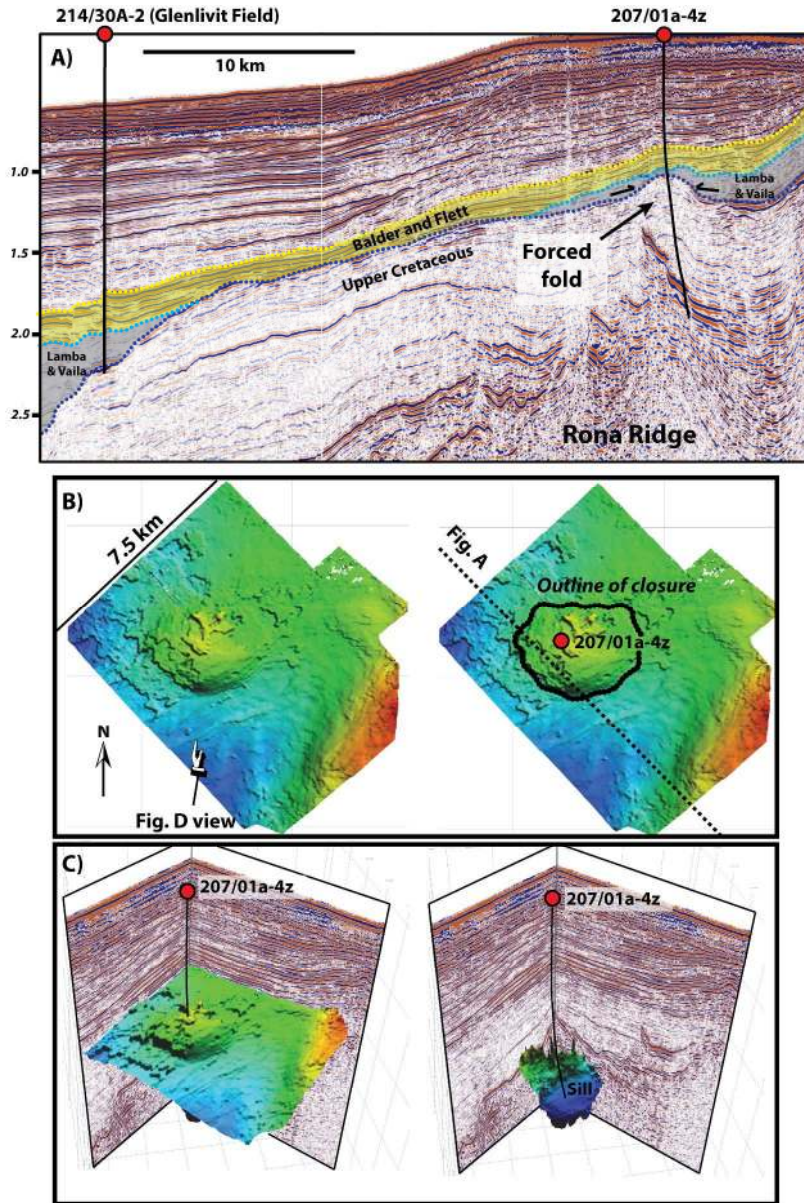


Fig 13
423x616mm (150 x 150 DPI)

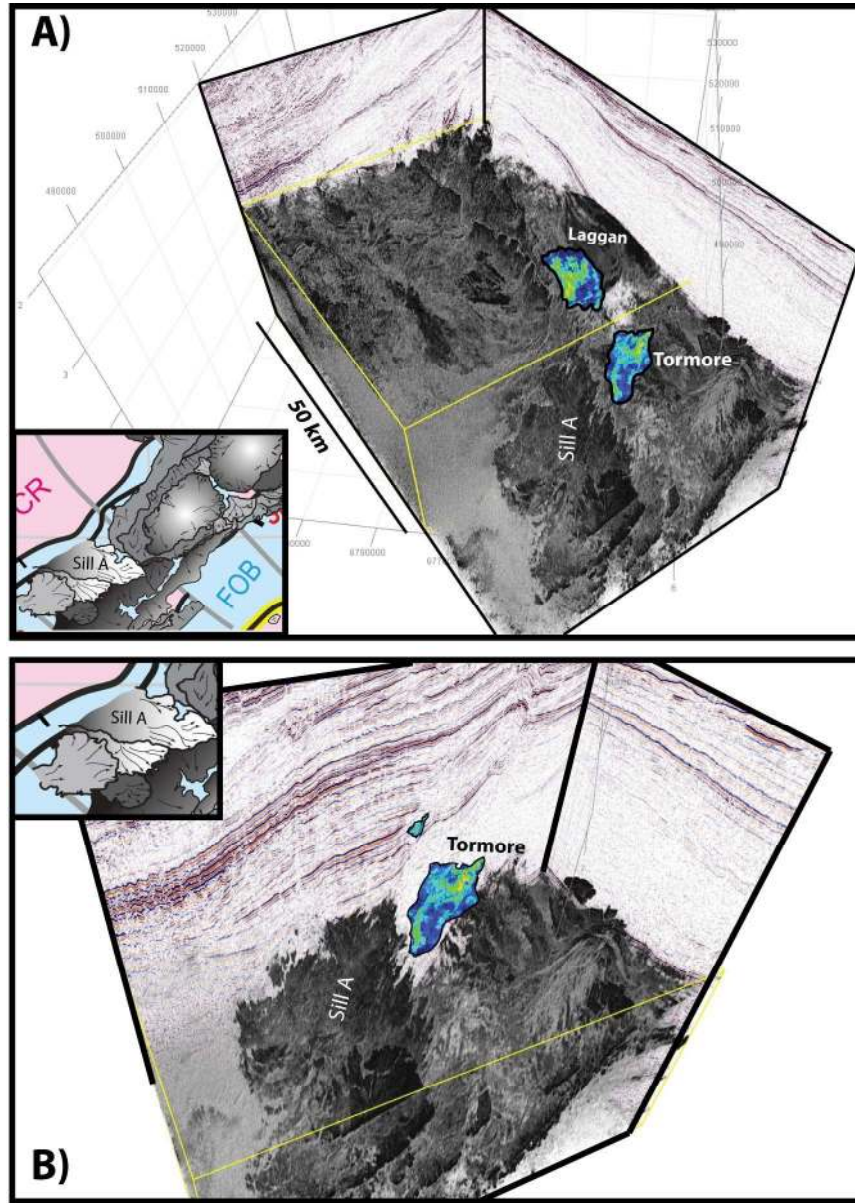


Fig 14
201x281mm (300 x 300 DPI)

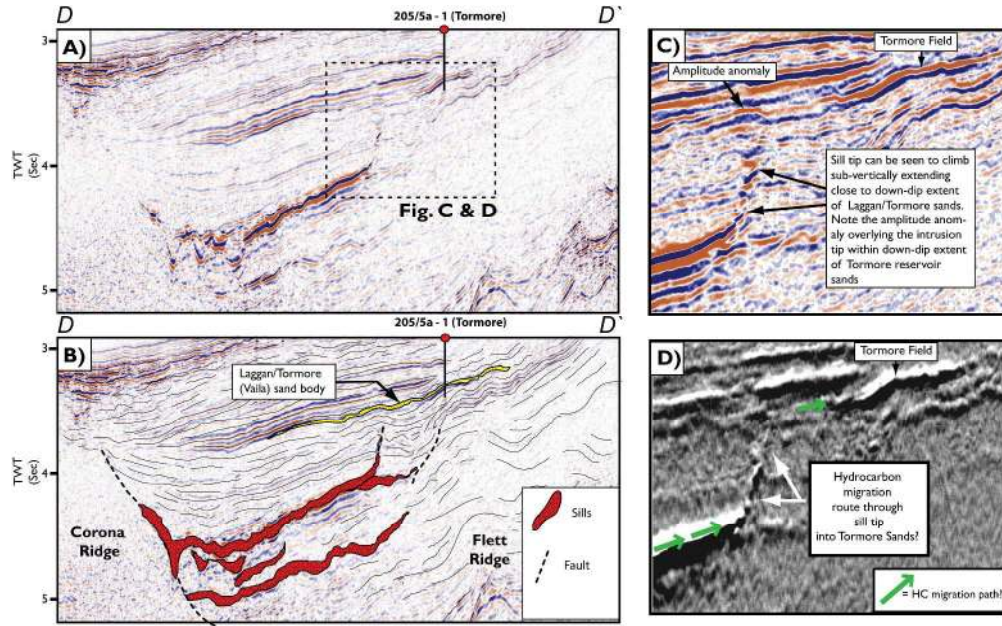


Fig 15
339x210mm (300 x 300 DPI)